

The universal rotation curve of dwarf disk galaxies

E.V. Karukes^{1,2*} P. Salucci^{1,2†}

¹*SISSA International School for Advanced Studies, Via Bonomea 265, 34136, Trieste, Italy*

²*INFN, Sezione di Trieste, Via Valerio 2, 34127, Trieste, Italy*

23 September 2016

ABSTRACT

We use the concept of the spiral rotation curves universality (see Persic et al. 1996) to investigate the luminous and dark matter properties of the dwarf disk galaxies in the local volume (size ~ 11 Mpc). Our sample includes 36 objects with rotation curves carefully selected from the literature. We find that, despite the large variations of our sample in luminosities (~ 2 of dex), the rotation curves in specifically normalized units, look all alike and lead to the lower-mass version of the universal rotation curve of spiral galaxies found in Persic et al. (1996).

We mass model $V(R/R_{opt})/V_{opt}$, the double normalized universal rotation curve of dwarf disk galaxies: the results show that these systems are totally dominated by dark matter whose density shows a core size between 2 and 3 stellar disk scale lengths. Similar to galaxies of different Hubble types and luminosities, the core radius r_0 and the central density ρ_0 of the dark matter halo of these objects are related by $\rho_0 r_0 \sim 100 M_\odot pc^{-2}$.

The structural properties of the dark and luminous matter emerge very well correlated. In addition, to describe these relations, we need to introduce a new parameter, measuring the compactness of light distribution of a (dwarf) disk galaxy. These structural properties also indicate that there is no evidence of abrupt decline at the faint end of the baryonic to halo mass relation. Finally, we find that the distributions of the stellar disk and its dark matter halo are closely related.

Key words:

galaxies: formation, galaxies: haloes, galaxies: kinematics and dynamics, dark matter, galaxies: dwarfs, galaxies: local volume

1 INTRODUCTION

It is widely believed that only 15 % of the total matter in the Universe is in form of ordinary baryonic matter. Instead the other 85 % is provided by dark matter (DM), which is detectable, up to now, only through its gravitational influence on luminous matter. The paradigm is that DM is made by massive gravitationally interacting elementary particles with extremely weak, if not null interaction via other forces (e.g., White & Negroponte 1982; Jungman et al. 1996). In this framework the well known (Λ)CDM scenario, successfully describing the large structure of the Universe, has emerged (Kolb & Turner 1990): accurate N-body simulations have found that the DM density profile of the virialized structures such as galactic halos is universal and well described by the Navarro-Frenk-White profile (hereafter NFW; Navarro et al. 1996b).

However, at the galactic scales, this scenario has significant challenges.

Firstly, the apparent mismatch between the number of the detected satellites around the Milky Way and the predictions of the corresponding simulations, known as the "missing satellite problem" (Klypin et al. 1999; Moore et al. 1999), which also occurs in the field galaxies (Zavala et al. 2009; Papastergis et al. 2011; Klypin et al. 2015). This discrepancy widens up when the masses of the detected satellites are compared to those of the predicted subhalos (i.e. "too big to fail problem") (see Boylan-Kolchin et al. 2012; Ferrero et al. 2012; Garrison-Kimmel et al. 2014; Papastergis et al. 2015).

Furthermore, there is the "core-cusp" controversy: the inner DM density profiles of galaxies generally appear to be cored, and not cuspy as predicted in the simplest (Λ)CDM scenario (e.g., Salucci 2001; de Blok & Bosma 2002; Gentile et al. 2005; Weinberg et al. 2013; Bosma 2004; Simon et al. 2005; Gentile et al. 2004, 2007; Donato et al. 2009; Oh et al. 2011, to name few).

* E-mail: ekarukes@sissa.it

† E-mail: paolo.salucci@sissa.it

These apparent discrepancies between the observations and the predictions of the DM-only simulations suggest to either abandon the (Λ)CDM scenario in favour of the others (e.g., selfinteracting DM [Vogelsberger et al. 2014](#); [Elbert et al. 2015](#) or warm DM [de Vega & Sanchez 2013](#); [de Vega et al. 2013](#); [Lovell et al. 2014](#); [de Vega et al. 2014](#)) or upgrade the role of baryonic physics in the galaxy formation process. The latter can be done including strong gas outflows, triggered by stellar and/or AGN feedback that are thought to strongly modify the original (Λ)CDM halo profiles out to a distance as large as the size of the stellar disk (e.g., [Navarro et al. 1996a](#); [Read & Gilmore 2005](#); [Mashchenko et al. 2006](#); [Pontzen & Governato 2012, 2014](#); [Di Cintio et al. 2014](#)).

Although these issues are present in galaxies of any luminosity, however in low luminosity systems they emerge more clearly and appear much more difficult to be resolved within the Λ CDM scenario. Galaxies with I-band absolute magnitude $M_I \gtrsim -17$ play a pivotal role in that, observationally, these objects are dark matter dominated at all radii. Moreover in the (Λ)CDM scenario they may be related to the building blocks of more massive galaxies. The importance of dwarf spheroidals in various DM issues is well known (see, e.g., [Gilmore et al. 2007](#)). However, down to $M_I \sim -11$ there is no shortage of rotationally supported late-type systems, although a systematic investigation is lacking. These rotationally supported systems have a rather simple kinematics suitable for investigating the properties of their dark matter content.

In normal spirals, one efficient way to represent and model their rotation curves (RCs) comes from the concept of a universal rotation curve (URC). Let us stress that the concept of universality in RCs does not mean that all of them have a unique profile, but that all the RCs of 10^9 local spirals (within $z \simeq 0.1$) can be described by a same function of radius, modulated by few free parameters. They depend on the galaxy's global properties, namely magnitude and a characteristic radius of the luminous matter¹ so that: $V(R) = V(R, M, R_{opt})$.

This concept, implicit in [Rubin et al. \(1985\)](#), pioneered by [Persic & Salucci \(1991\)](#), set by [Persic et al. \(1996\)](#) (PSS, Paper I) and extended to large galactocentric radii by [Salucci et al. \(2007\)](#) has provided us the mass distribution of (normal) disk galaxies in the magnitude range $-23.5 \lesssim M_I \lesssim -17^2$. This curve, therefore, encodes all the main structural properties of the dark and luminous matter of every spiral (PSS, [Yegorova & Salucci 2007](#)). In this paper, we work out to extend the RCs universality to dwarf systems and then, to use it to investigate the DM distribution in dwarf disk galaxies.

Noticeably, for this population of galaxies the approach of stacking the available kinematics is very useful. In fact, presently, for disk systems with the optical velocity $V_{opt} \lesssim 61 \text{ km/s}$, some kinematical data have become available. However, still there are not enough individual *high quality high resolution extended* RCs to provide us with a solid knowledge of their internal distribution of mass. Instead, we will prove

that the 36 selected in literature *good quality good resolution reasonably extended* RCs (see below for these definitions), once coadded, provide us with a reliable kinematics yielding to their mass distribution.

In this work, we construct a sample of dwarf disks from the local volume catalog (LVC) ([Karachentsev et al. 2013](#), hereafter K13), which is $\sim 70\%$ complete down to $M_B \approx -14$ and out to 11 Mpc, with the distances of galaxies obtained by means of primary distance indicators.

Using LVC, we go more than 3 magnitudes fainter with respect to the sample of spirals of PSS. Moreover the characteristics of the LVC guarantee us against several luminosity biases that may affect such faint objects. The total number of objects in this catalog is ~ 900 of which ~ 180 are dwarf spheroidal galaxies, ~ 500 are dwarf disk galaxies and the rest are ellipticals and spirals.

All our galaxies are low mass bulgeless systems in which rotation, corrected for the pressure support, totally balances the gravitational force. Morphologically, they can be divided into two main types: gas-rich dwarfs that are forming stars at a relatively-low rate, named irregulars (Irrs) and starbursting dwarfs that are forming stars at an unusually high rate, named blue compact dwarfs (BCD). The dwarf Irr galaxies are named "irregulars" due to the fact that they usually do not have a defined disk shape and the star formation is not organized in spiral arms. However, some gas-rich dwarfs can have diffuse, broken spiral arms and be classified as late-type spirals (Sd) or as a Magellanic spiral (Sm). The starbursting dwarfs are classified as BCD due to their blue colours, high surface brightness and low luminosities. Notice that it is not always easy to distinguish among these types since the galaxies we are considering often share the same parameters space for many structural properties (e.g., [Kormendy 1985](#); [Binggeli 1994](#); [Tolstoy et al. 2009](#)).

In this paper, we neglect the morphology of the baryonic components as long as their stellar disk component follows a radially exponential surface density profile; the identifiers of a galaxy are V_{opt} , its disk length scale R_D and its K-band magnitude M_K that can be substituted by its disk mass. We refer to these systems of any morphologies and $M_K \gtrsim -18$ as dwarf disks (dd).

In order to compare galaxy luminosities in different bands, we write down the dd relation between the magnitudes in different bands $< B - K > \simeq 2.35$ ([Jarrett et al. 2003](#)) and $< B - I > \simeq 1.35$ ([Fukugita et al. 1995](#)).

The plan of this paper as follows: in Section 2 we describe the sample that we are going to use; in Section 3 we introduce the analysis used to build the synthetic RC; in Section 4 we do the mass modelling of the synthetic RC; in Section 5 we denormalize the results of the mass modelling in order to describe individually our sample of galaxies and then we define their scaling relations; in Section 6 we discuss our main results.

2 THE SAMPLE

We construct our dwarf disk galaxy sample out of the LVC ([Karachentsev et al. 2013](#)) by adopting the following 4 selection criteria:

1. We include disk galaxies with the optical velocity less

¹ i.e. optical radius R_{opt} defined as the radius encompassing 83 % of the total luminosity.

² Extensions of the URC to other Hubble types are investigated in [Salucci & Persic \(1997\)](#); [Noordermeer et al. \(2007\)](#).

Table 1. Sample of dwarf disk galaxies. Columns: **(1)** galaxy name; **(2)** galaxy distance; **(3)** rotation curve source; **(4)** exponential scalelength of a galaxy stellar disk; **(5)** disk scalelength source; **(6)** rotation velocity at the optical radius; **(7)** absolute magnitude in K-band.

Name	D	RCs refs	R_D	R_D refs	V_{opt}	M_K
—	Mpc	—	kpc	—	km/s	mag
(1)	(2)	(3)	(4)	(5)	(6)	(7)
H_α ; HI						
UGC1281	4.94	1; 2	0.99	a	53.8	-17.97
UGC1501	4.97	1; -	1.32	a	50.2	-18.19
UGC5427	7.11	1; -	0.38	e	54.0	-17.06
UGC7559	4.88	-; 2, 3	0.88	b	37.4	-16.91
UGC8837	7.21	-; 2	1.55	b	47.6	-18.25
UGC7047	4.31	-; 2, 4	0.57	c	37.0	-17.41
UGC5272	7.11	-; 2	1.28	b	55.0	-16.81
DDO52	10.28	-; 3	1.30	b	60.0	-17.69
DDO101	16.1	-; 3	0.94	b	58.8	-19.01
DDO154	4.04	-; 3	0.75	b	38.0	-15.70
DDO168	4.33	-; 3	0.83	b	60.0	-17.07
Haro29	5.68	-; 3, 4	0.28	b	32.6	-16.26
Haro36	8.9	-; 3	0.97	h	56.5	-17.63
IC10	0.66	-; 3	0.38	b	41.0	-17.59
NGC2366	3.19	-; 3, 4	1.28	b	55.0	-18.38
WLM	0.97	-; 3	0.55	b	33.0	-15.93
UGC7603	8.4	-; 2	1.11	2	60.3	-19.07
UGC7861	7.9	-; 5	0.62	i	61.0	-19.74
NGC1560	3.45	-; 6	1.10	6	56.1	-18.43
DDO125	2.74	1; 2	0.49	c	17.0	-16.96
UGC5423	8.71	1; 3	0.52	d	27.5	-17.71
UGC7866	4.57	-; 2	0.54	2	28.7	-17.18
DDO43	5.73	-; 2	0.57	b	35.3	-15.72
IC1613	0.73	-; 3	0.60	b	19.0	-16.89
UGC4483	3.21	-; 4	0.16	f	20.8	-14.20
KK246	7.83	-; 9	0.58	9	34.6	-16.17
NGC6822	0.5	-; 10	0.56	b	35.0	-17.50
UGC7916	9.1	-; 2	1.63	h	37.0	-16.22
UGC5918	7.45	-; 2	1.23	2	45.0	-17.50
AndIV	7.17	-; 11	0.48	11	32.2	-14.78
UGC7232	2.82	-; 2	0.21	f	37.0	-16.46
DDO133	4.85	-; 3	0.9	g	42.4	-17.31
UGC8508	2.69	1; 3	0.28	j	25.5	-15.58
UGC2455	7.8	-; 2	1.06	h	47.0	-19.91
NGC3741	3.03	-; 7	0.18	c	22.0	-15.15
UGC11583	5.89	-; 8	0.17	8	52.2	-16.55

Notes. RC & R_D references: Moiseev (2014)-1, Swaters et al. (2009)-2, Oh et al. (2015)-3, Lelli et al. (2014)-4, Epinat et al. (2008)-5, Gentile et al. (2010)-6, Gentile et al. (2007)-7, Begum & Chengalur (2004)-8, Gentile et al. (2012)-9, Weldrake et al. (2003)-10, Karachentsev et al. (2016)-11, van Zee (2001)-a, Hunter & Elmegreen (2004)-b, Sharina et al. (2008)-c, Parodi et al. (2002)-d, Simard et al. (2011)-e, Martin (1998)-f, Hunter et al. (2011)-g, Herrmann et al. (2013)-h, Yoshino & Yamauchi (2015)-i, Hunter et al. (2012)-j. Distance D and absolute magnitude in K-band M_K are taken from Karachentsev et al. (2013).

than ~ 61 km/s (disk systems with larger velocity amplitude are studied in PSS);

2. The rotation curves extend to at least 3.2 disk scale lengths³. However, we allowed ourselves to extrapolate modestly the RCs of UGC1501, UGC8837, UGC5272 and IC10 due to their smoothness;

3. The RCs are symmetric, smooth and with an average internal uncertainty less than 20 %;

4. The galaxy disk length scale R_D and the inclination function $1/\sin i$ are known within 20 % uncertainty.

It is worth noticing that for a RC to fulfil criteria (2), (3) and (4) it is sufficient to qualify it for the *coaddition* pro-

cedure but not necessarily this is the case for the *individual* modelling.

The kinematical data used in our analysis are HI and H_α rotation curves available in the literature (see Table 1), which are corrected for inclination and instrumental effects. Furthermore, circular velocities of low mass galaxies, with $V_{max} \lesssim 50$ km/s, require to be checked for the pressure support correction, this can be done using the so-called "asymmetric drift correction" (Dalcanton & Stilp 2010). Therefore, most of the RCs in our sample either have the asymmetric drift correction applied (the ones taken from Oh et al. 2011, 2015; Lelli et al. 2014; Gentile et al. 2010, 2012) or pressure support has been determined and is too small to affect the RC (the ones taking from Swaters et al. 2009; Weldrake et al. 2003; Karachentsev et al. 2016). Despite that, we leave three

³ $R_{opt} \simeq 3.2R_D$

galaxies (UGC1501, UGC5427 and UGC7861) for which circular velocities were not corrected. In view of their V_{max} are larger than 50 km/s, therefore the effect should be minor. In the innermost regions of galaxies, when available, we use also H_α data not corrected for the asymmetric drift since such term is negligible as it was pointed out by e.g. [Swaters et al. \(2009\)](#); [Lelli et al. \(2012\)](#).

We stress that the above selection process has left out few objects whose RCs are sometimes considered in literature, e.g. the RC of DDO 70 described by [Oh et al. \(2015\)](#) has failed our criteria (3) because of its abnormal shape. Our approach stands firmly that, in order to provide us with proper and correct information about a galaxy dark and luminous mass distribution, the relative kinematical and the photometric data must reach a well defined level of quality, otherwise they will be confusing rather than enlightening the issue.

Therefore, we ended with the final sample of 36 galaxies spanning the magnitude and disk radii intervals, $-19 \lesssim M_I \lesssim -13$, $0.18 \text{ kpc} \lesssim R_D \lesssim 1.63 \text{ kpc}$ and the optical velocities $17 \text{ km/s} \lesssim V_{opt} \lesssim 61 \text{ km/s}$ (see Table 1, the references for HI and H_α RCs of our sample are also given in the table and the individual RCs are plotted in Fig. A of Appendix A).

The log average optical radius $\langle R_{opt} \rangle$ and the log average optical velocity $\langle V_{opt} \rangle$ are 2.5 kpc, 39.6 km/s, respectively, (these values will be specifically needed in Section 5). For a comparison, the galaxy sample of PSS spans the magnitude interval $-23.5 \lesssim M_I \lesssim -17$, the disk scale radii $2 \text{ kpc} \lesssim R_D \lesssim 30 \text{ kpc}$, and the optical velocities between 70 km/s and 300 km/s. Therefore, our sample will extend the URC of PSS by more than 2 orders of magnitudes down in galaxy luminosity.

3 THE URC OF DWARF DISKS

First, we plot the RCs of galaxies in our sample expressed in physical units in log-log scales (see the left panel of Fig. 1). We realize, even at a first glance, that, contrary to the RCs of normal spirals (e.g., [Yegorova & Salucci 2007](#), PSS), each dd galaxy has a RC with a very different profile, as it has also been noticed by [Oman et al. \(2015\)](#). All curves are rising with radius but at a very different place.

Surprisingly, the origin of such diversity is closely linked with the very large scatter that the dds show in the relationship between the optical radius R_{opt} and the luminosity L_K shown in Fig. 2. In our sample the relation still holds but the scatter remarkably increased, while in normal spirals luminosities and disk sizes are very well correlated.

Thus, also in dwarf disk galaxies, by following the analogous PSS procedure, we derive a universal profile of their RCs. As an initial step of the co-addition procedure (see PSS for details) each of the 36 $V(R)$ has been normalized to its own optical radius R_{opt} and to its optical velocity V_{opt} obtained by RC data interpolation. We then derive the quantity $V(R/R_{opt})/V(R_{opt})$. This double normalization eliminates most of the small scale individualities of the RCs.⁴ It

can be seen in the right panel of Fig. 1 that as a consequence of the double normalization, all RCs have become similar to each other, leading to a profile very similar to that coadded of the least luminous normal spirals (red joined circles of Fig. B.1).

This effect is not new: in [Verheijen & de Blok \(1999\)](#); [Salucci & Persic \(1997\)](#) (see also [McGaugh 2014](#)) the variety of RCs shapes in physical units between high surface brightness galaxies and LSB objects of similar maximum velocities was eliminated by normalizing $V(R)$ on the corresponding disk scale lengths.

In investigating our sample RC profiles we will construct just one luminosity bin, because of the data limitation. At its support, let us note that the URC at low luminosities converges to a profile independently of luminosity. The double normalized velocity data are co-added as follows: we set 14 radial bins in the position r_i ⁵ given by the vertical dashed grey lines in Fig. 3 and reported in Table 2. Each bin is equally divided in two, we adopt that every RC can contribute to each of the 28 semi bins only with one data point. When, for a RC more data points concurring to the same semi bin, these are averaged accordingly. The last bin is set at $r_i = 1.9$ due to the lack of outer data.

Since a galaxy cannot contribute more than twice to every bin i , each of them, centred at r_i (see Table 2) and with boundaries shown in Fig. 3, has a number N_i data (see Table 2) which runs from a maximum of 68 and a minimum that we have set to be 14. Then, from N_i data in each radial bin i we compute the average weighted rotation velocity, where the weights are taken from the uncertainties in the rotation velocities (given online).

In Table 2 we report the 14 r_i positions, the values of the coadded double normalized curve $v = V(R/R_{opt})/V(R_{opt})$ and of their uncertainties dv , calculated as the standard deviation with respect to the mean⁶. The universality of this curve can be inferred from its very small r.m.s. values (see Fig. 3). Furthermore, we investigate the universality in deep by calculating the residuals of each individual RC with respect to the emerging coadded curve (Table 2 column 5):

$$\chi^2 = \frac{\sum_{ij} \frac{(v_{ij} - v_i)^2}{\delta_{ij}^2}}{N}, \quad (1)$$

where v_{ij} are the individual RC data referring to the bin i of the double normalized RC of the j dwarf disk (j from 1 to 36), v_i is the double normalized coadded i value (i from 1 to 14) (see Fig. 3), δ_{ij} are the observational errors of the normalized circular velocities and N is the total number of the data points ($N = 350$)⁷.

We consider the 14 v_i as an exact numerical function which we attempt to fit with double normalized velocity data v_{ij} : we found that the fit is excellent, the reduced chi-square is ~ 1.0 and the reduced residuals $dv_{ij} = v_{ij} - v_i$ are very small, see Fig. 4. In fact $\sim 72\%$ of the residuals is smaller

⁴ The double normalization refers to both quantities plotted on the X axis and Y axis of Fig. 3.

⁵ Calculated as a mean value in a bin.

⁶ Lowercase letters refer to normalized values, while capital letters to the values in physical units.

⁷ i is the index number of a radial bin and ij are the index numbers of a data j in a bin i .

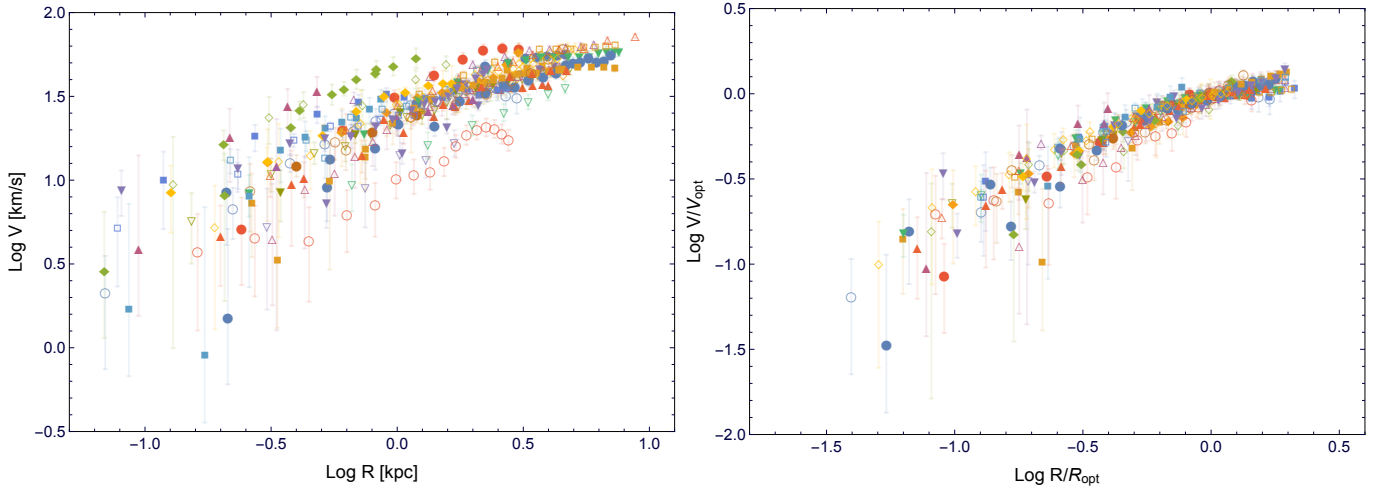


Figure 1. Individual RCs. *Left panel:* in physical units. *Right panel:* after double normalization on R_{opt} and V_{opt} .

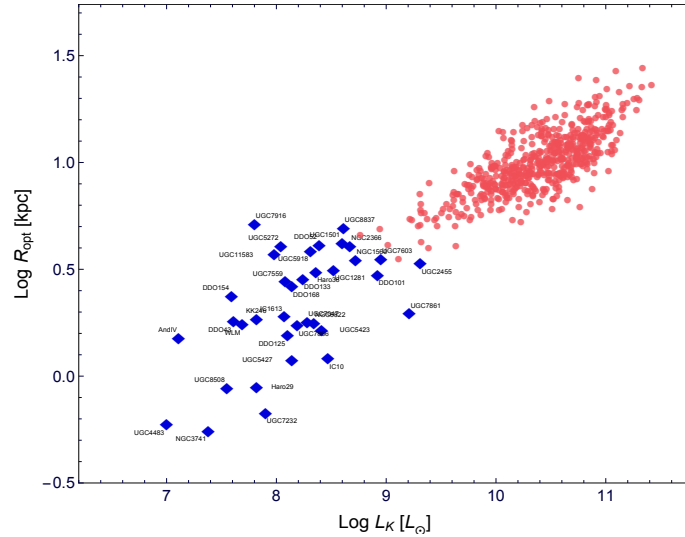


Figure 2. The optical radius versus the total luminosity. Red circles indicate the normal spiral galaxies from the sample of PSS and blue diamonds are the dwarf galaxies of the present work.

than 1 δ_{ij} , $\sim 26\%$ falls inside 3 δ_{ij} and only the remaining $\sim 2\%$ is anomalously large.

Finally, in order to check the existence of biases, we investigate, in all 14 bins, whether the dv_{ij} residuals have any correlation with the optical velocity $\log V_{opt}^{ij}$ of the corresponding galaxy (see Fig. 5). However, we did not find any correlation, see Fig. 5; dd galaxies of any luminosity (and V_{opt}) show the same double normalized RC profile. In fact, our accurate analysis shows no evidence of dd with a double normalized RC relevantly different from the coadded $v_i(r_i)$ derived in this section and given in Table 2.

It is worth to compare the present results with those of PSS; in the left panel of Fig. B.1 the former is plotted alongside with the similar curve of the PSS's lowest luminosity bin (see also Fig. 6 in PSS). The latter contains 40 normal spirals with the average I-band magnitude of $\langle M_I \rangle = -18.5$. Noticeably, the two double normalized coadded RCs are in good agreement, keeping in mind that, in the present work,

the luminosity bin $-19 \lesssim M_I \lesssim -13$ is as big as the whole luminosity range of PSS (right panel of Fig. B.1) that, instead, was divided in 11 bins.

Thus, starting from $M_I \sim -18$ and down to the faintest systems, the mass structure of disk galaxies is just a dark halo with a density core radius as big as the stellar disk. At $M_I \gtrsim -18.5$ the stellar disk contribution disappears and, remarkably, the RC profile becomes solid body like: $V(R) \propto R$.

We now investigate quantitatively the last statement: one can notice that the coadded RC of dwarf disks is slightly shallower than that of the least luminous spirals of PSS (see left panel of Fig. B.1 and Appendix B). Therefore, we check for the presence of any trend between luminosity and shape of the corresponding RC inside our sample of 36 dwarf disks. We divide them in 3 subsamples (12 galaxies each, ordered by their luminosity). Then, we derive the 3 corresponding stacked RCs (see Table B1). No trend between RC shape

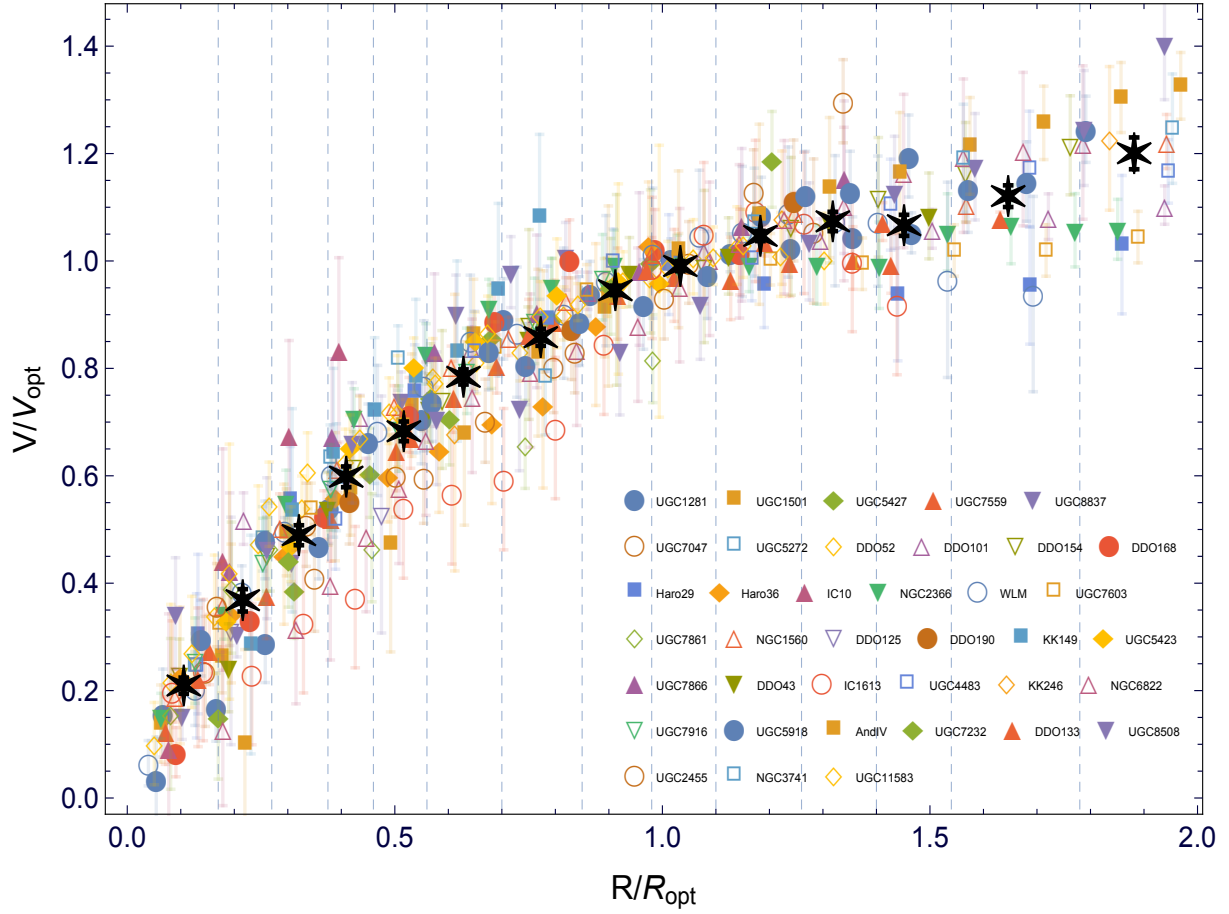


Figure 3. Individual RCs normalized to R_{opt}, V_{opt} . Black stars indicate the synthetic RC. Bins are shown as vertical dashed grey lines.

Table 2. Data in the radial bins. Columns: (1) bin number; (2) number of data points; (3) the central value of a bin; (4) the average coadded weighted normalized rotation velocity; (5) r.m.s. on the average coadded rotation velocity (6) denormalized on $\langle R_{opt} \rangle$ values of radii, *kpc* (7) denormalized on $\langle V_{opt} \rangle$ values of velocities, *km/s* (8) r.m.s. on the denormalized rotation velocity.

i	N	r_i	v_i	dv_i	R_i	V_i	dV_i
(1)	(2)	(3)	(4)	(5)	(6)	(7)	(8)
1	31	0.11	0.21	0.015	0.27	8.28	0.59
2	30	0.22	0.37	0.021	0.54	14.57	0.82
3	21	0.32	0.49	0.019	0.81	19.37	0.74
4	26	0.41	0.60	0.019	1.03	23.68	0.78
5	25	0.52	0.68	0.018	1.30	27.03	0.72
6	33	0.63	0.78	0.014	1.58	31.04	0.56
7	34	0.77	0.86	0.016	1.94	34.0	0.63
8	28	0.91	0.95	0.009	2.29	37.42	0.35
9	25	1.03	0.99	0.009	2.60	39.21	0.37
10	28	1.18	1.05	0.010	2.97	41.43	0.38
11	18	1.32	1.07	0.018	3.31	42.50	0.71
12	17	1.45	1.07	0.020	3.65	42.22	0.78
13	20	1.65	1.12	0.020	4.13	44.37	0.80
14	14	1.88	1.20	0.030	4.73	47.53	1.17

and luminosity was found, differently from what it occurs for spirals of higher luminosity, see Appendix B and Fig B.1.

Finally, let us point out that neither the double normalization, nor the stacking of our 36 objects is the cause of the solid body profile of the RC in Fig. 3 and Table 2. The

reason is that each RC of our sample, also when considered in physical units, shows, inside $2R_D$, a solid body profile

Therefore, we conclude the existence of the coadded RC for the dd population. This is the first step to obtain that the kinematics of dd galaxies can be described by a smooth universal function, exactly as it happens in normal spirals (PSS, Salucci et al. 2007).

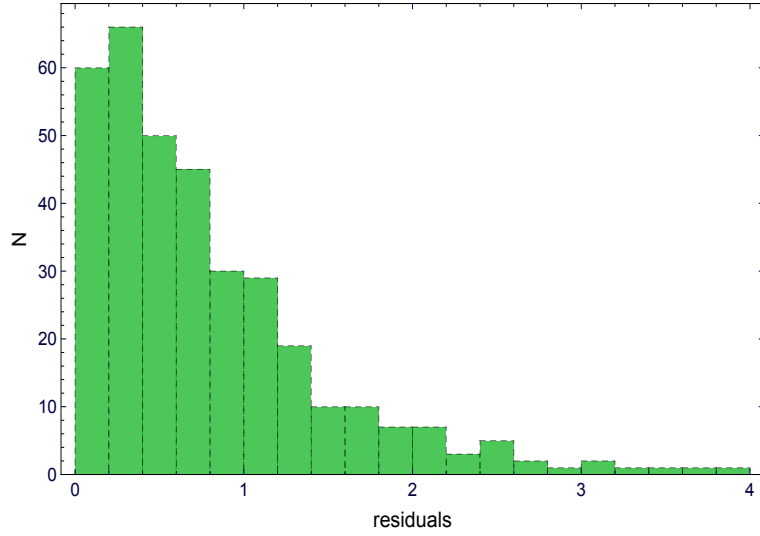


Figure 4. The distribution of residuals in terms of rms, which are listed in column 5 of Table 2.

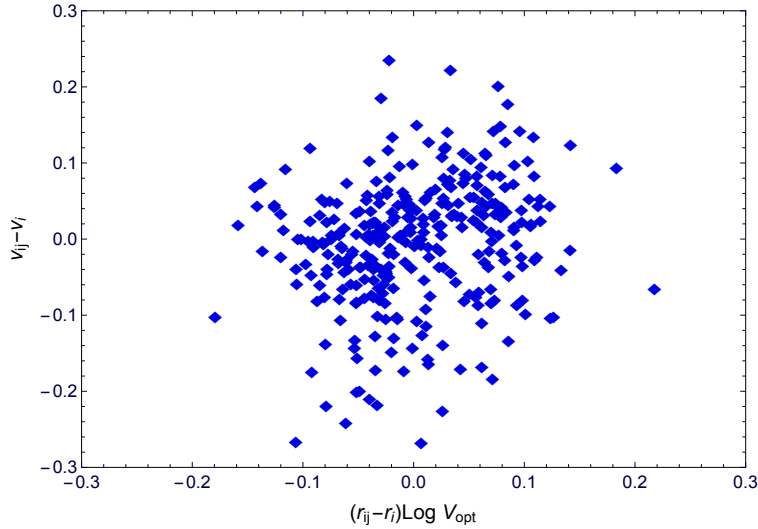


Figure 5. The v_{ij} residuals in the 14 bins versus the optical velocity $\log V_{opt}$. Coefficient of correlation R^2 is ~ 0.06 .

4 MODELLING THE DOUBLE NORMALIZED COADDED RC OF DWARF DISK GALAXIES

As in normal spirals (see PSS) we mass model the coadded RC data that represent the whole kinematics of dds. More precisely,

1. the coadded (double normalized) RC (see Table 2), once proven to be universal, is the basic data with which we build the mass model of dwarf disk galaxies;

2. for simplicity, we rescale the 14 normalized velocities v_i to the log average values of the sample $\langle V_{opt} \rangle$ and $\langle R_{opt} \rangle$, 39.6 km/s and 2.1 kpc, respectively. In details, we write:

$$\begin{aligned} \langle V_i \rangle &= v_i \langle V_{opt} \rangle; \\ \langle R_i \rangle &= r_i \langle R_{opt} \rangle, \end{aligned} \quad (2)$$

the 14 values of $\langle V_i \rangle$ and $\langle R_i \rangle$ are also reported in Table 2 (columns 6-7), where angle brackets indicate normalization to the log average values of optical radius and optical ve-

locity. This RC is the fiducial curve for dwarf disk systems. In fact, we take the coadded curve Table 2 (columns 3-5) and we apply it to a galaxy with the values of R_{opt} and V_{opt} equal to the average values in our sample. Since all dd RCs have the same double normalized profile, the parameters of the resulting mass model can be easily rescaled back to cope with galaxies of different V_{opt} and R_{opt} .

The fiducial rotation curve (Table 2 columns 6-8) of dwarf disks consists of 14 velocity data points extended out to $1.9 \langle R_{opt} \rangle$. The uncertainties on the velocities are at the level of $\sim 3\%$ (see Fig 3).

The circular velocity model $V_{tot}(R)$ consists into the sum, in quadrature, of three terms V_D, V_{HI}, V_{DM} that describe the contribution from the stellar disk, the HI disk and dark halo and that must equate to the observed circular velocity:

$$V_{tot}^2(R) = V_m(R) \equiv V_D^2(R) + V_{HI}^2(R) + V_{DM}^2(R). \quad (3)$$

Notice that in the RHS of eq. 3, we have neglected the stellar bulge contribution that is, in fact, absent in dds.

4.1 Stellar component

With a constant stellar mass to light ratio as function of radius (see e.g. [Bell & de Jong 2001](#)) all 36 dds have the same surface density stellar profile Σ_D well represented by the Freeman disk ([Freeman 1970](#)):

$$\Sigma_D(R) = \frac{M_D}{2\pi R_D^2} e^{-\frac{R}{R_D}} \quad (4)$$

then, the contribution of the stellar disk $V_D(R)$ is

$$V_D^2(R) = \frac{1}{2} \frac{GM_D}{R_D} (3.2x)^2 (I_0 K_0 - I_1 K_1), \quad (5)$$

where $x = R/R_{opt}$ and I_n and K_n are the modified Bessel functions computed at 1.6 x.

4.2 Gas disk

For each galaxy the gaseous mass M_{HI} was taken from K13, log averaged and then multiplied by a factor 1.33 to account for the He abundance, then we obtain $\langle M_{HI} \rangle = 1.7 \times 10^8 M_\odot$. The HI surface density profile is not available for all dwarf disk galaxies of our sample, therefore we model it, by following [Tonini et al. \(2006\)](#), as a Freeman distribution with a scale length three times larger that of the stellar disk $\Sigma_{HI}(R) = \frac{M_{HI}}{2\pi(3R_D)^2} e^{-\frac{R}{3R_D}}$, then, the contribution of the gaseous disk $V_{HI}(R)$ is

$$V_{HI}^2(R) = \frac{1}{2} \frac{GM_{HI}}{3R_D} (1.1x)^2 (I_0 K_0 - I_1 K_1), \quad (6)$$

where $x = R/R_{opt}$ and I_n and K_n are the modified Bessel functions computed at 0.53 x.

This scheme is fairly well supported in dds for which the HI surface density data are available (e.g., data from [Oh et al. 2015](#); [Gentile et al. 2010, 2012](#)). In order to clarify the latter, we plot in Fig. 6, alongside the observed RC of HI component and our approximation of the HI distribution for 5 galaxies of our sample.

In addition, let us stress that the gas contribution is always a minor component to the dds circular velocities, so that, possible errors in its estimate do not alter the mass modelling neither affect any result of this paper.

4.3 Dark halo

Many different halo radial mass profiles have been proposed over the years. Thus, in this work we are going to test the following profiles.

4.3.1 Burkert profile

The URC of normal spirals and the kinematics of individual objects ([Salucci & Burkert 2000](#)) point to dark halos density profiles with a constant core, and, in particular, to the Burkert halo profile ([Burkert 1995](#)), for which:

$$\rho_{B,URC}(r) = \frac{\rho_0 r_c^3}{(r + r_c)(r^2 + r_c^2)}, \quad (7)$$

where ρ_0 (the central density) and r_c (the core radius) are the two free parameters and $\rho_{B,URC}$ means that we have adopted the Burkert profile for the URC DM halo component. Hereafter, we will freely exchange the two denominations according to the issue considered.

Adopting spherical symmetry, the mass distribution of the Burkert halos is given by:

$$M_{URC}(r) = 2\pi\rho_0 r_c^3 \left[\ln\left(1 + \frac{r}{r_c}\right) - \frac{r}{r_c} \ln\left(\frac{r}{r_c}\right) + 0.5 \ln\left(1 + \left(\frac{r}{r_c}\right)^2\right) \right] \quad (8)$$

4.3.2 NFW profile

We will investigate also NFW profile. [Navarro et al. \(1996b\)](#) found, in numerical simulations performed in the (Λ) CDM scenario of structure formation, that virialized systems follow a universal dark matter halo profile. This is written as:

$$\rho_{NFW}(r) = \frac{\rho_0}{\left(\frac{r}{r_s}\right)\left(1 + \frac{r}{r_s}\right)^2}, \quad (9)$$

where ρ_0 and r_s are, respectively, the characteristic density and the scale radius of the distribution. These two parameters can be expressed in terms of the virial mass $M_{vir} = 4/3\pi 100\rho_{crit} R_{vir}^3$, the concentration parameter $c = \frac{R_{vir}}{r_s}$ and the critical density of the Universe $\rho_{crit} = 9.3 \times 10^{-30} g\ cm^{-3}$. By using eq.(9), we can write:

$$\begin{aligned} \rho_0 &= \frac{100}{3} \frac{c^3}{\log(1+c) - \frac{c}{1+c}} \rho_{crit} \quad g\ cm^{-3}; \\ r_s &= \frac{1}{c} \left(\frac{3 \times M_{vir}}{4\pi 100\rho_{crit}} \right)^{1/3} \quad kpc. \end{aligned} \quad (10)$$

Then, the RC curve for the NFW DM profile is

$$V_{NFW}^2(r) = V_{vir}^2 \frac{\log(1+cx) - cx/(1+cx)}{x[\log(1+c) - c/(1+c)]}, \quad (11)$$

where $x = r/R_{vir}$ and V_{vir} represents the circular velocity at R_{vir} .

Let us point out that, within the (Λ) CDM scenario, the NFW profile maybe not the present days dark halos around spirals. Baryons, during the formation of the stellar disks, may have been able to modify the original DM density distributions (see, e.g., [Pontzen & Governato 2012, 2014](#); [Di Cintio et al. 2014](#)). We then consider eq. (11) as the fiducial profile of (Λ) CDM scenario, a working assumption useful to frame changes of the latter.

4.3.3 DC14 profile

A solution for the existence of cored profiles in (Λ) CDM scenario may have emerged by considering the recently developed DM density profile (see [Di Cintio et al. 2014](#)). This profile (hereinafter referred to as DC14) accounts for the effects of feedback on the DM halos due to gas outflows generated in high density starforming regions during the history

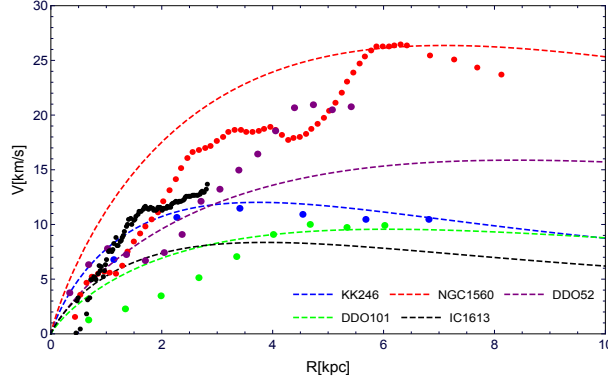


Figure 6. The observed circular velocities of HI taking from Gentile et al. (2010, 2012); Oh et al. (2015) (points) and the approximation for the distribution of HI component as described in Tonini et al. (2006) (dashed lines).

of the stellar disk. The resulting radial profile is far from simple, since it starts from an (α, β, γ) double power-law model (see Di Cintio et al. 2014)

$$\rho_{DC14}(r) = \frac{\rho_s}{\left(\frac{r}{r_s}\right)^\gamma \left(1 + \left(\frac{r}{r_s}\right)^\alpha\right)^{\frac{(\beta-\gamma)}{\alpha}}} \quad (12)$$

where ρ_s is the scale density and r_s the scale radius. The inner and the outer regions have logarithmic slopes $-\gamma$ and $-\beta$, respectively, and α indicates the sharpness of the transition. These three parameters are fully constrained in terms of the stellar-to-halo mass ratio as shown in Di Cintio et al. (2014):

$$\begin{aligned} \alpha &= 2.94 - \log_{10}[(10^{X+2.33})^{-1.08} + (10^{X+2.33})^{2.29}] \\ \beta &= 4.23 + 1.34X + 0.26X^2 \\ \gamma &= -0.06 + \log_{10}[(10^{X+2.56})^{-0.68} + (10^{X+2.56})] \end{aligned} \quad (13)$$

$$\text{where } X = \log_{10} \left(\frac{M_D}{M_{halo}} \right).$$

Then, using the definition of the enclosed mass, we can write down the expression for the scale density of the DC14 profile:

$$\rho_s = M_{vir}/4\pi \int_0^{R_{vir}} \frac{r^2}{\left(\frac{r}{r_s}\right)^\gamma \left[1 + \left(\frac{r}{r_s}\right)^\alpha\right]^{\frac{\beta-\gamma}{\alpha}}} dr. \quad (14)$$

Finally, by combining the above eqs. (12-14) we obtain a density profile as a function of three parameters r_s , M_{halo} and M_D , which we use in order to define the RC curve for the DC14 DM profile.

Despite the complexity of the proposed scheme, it is worth to test such DM density profile based on the analysis of hydro-dynamically simulated galaxies (see Di Cintio et al. 2014) drawn from the MaGICC project (Brook et al. 2012; Stinson et al. 2013).

4.4 Results

In Fig. 7 we show that the modelling of the fiducial RC by means of the dwarf disk universal rotation curve (ddURC) mass model: an exponential Freeman disk, a gaseous disk plus a Burkert halo profile. This result is very successful

(see Fig. 4) with $\chi_{red}^2 < 1$. The best-fit parameters of the fiducial RC are:

$$\begin{aligned} \log\langle\rho_0\rangle &= 7.53 \pm 0.04 \quad M_\odot \text{ kpc}^{-3}; \\ \langle r_c \rangle &= 2.34 \pm 0.14 \quad \text{kpc}; \\ \log\langle M_D \rangle &= 7.72 \pm 0.15 \quad M_\odot. \end{aligned} \quad (15)$$

The resulting virial mass is $\langle M_{vir} \rangle = (1.38 \pm 0.05) \times 10^{10} M_\odot$. Note that quite large fitting uncertainties in the estimate of the stellar disk masses come from the fact that the stellar disks are subdominant components in these galaxies.

It is worth to recall that the coadded double normalized RC of dds (Table 2 columns 3-5) would be identically well fitted and the relative structure parameters can easily be obtained via the transformation laws in eq. (2).

NFW profile fails to reproduce the synthetic RC (see Fig. 7), the reduced chi-square is ≈ 12 and the best-fit parameters

$$\begin{aligned} \log\langle M_{vir} \rangle &= 11.74 \pm 0.94 \quad M_\odot; \\ \langle c \rangle &= 4.46 \pm 3.19; \\ \log\langle M_D \rangle &= 2.60_{-2.60}^{+?} \quad M_\odot. \end{aligned}$$

lead to totally unrealistic estimates of the stellar disk and halo masses.

The DC14 profile shows the same good quality fit (see Fig. 7) as the URC profile with $\chi_{red}^2 < 1$ and quite similar values of the structural parameters

$$\begin{aligned} \log\langle M_{vir} \rangle &= 10.29 \pm 0.02 \quad M_\odot; \\ \langle r_s \rangle &= 2.09 \pm 0.14; \\ \log\langle M_D \rangle &= 7.27 \pm 0.14 \quad M_\odot. \end{aligned}$$

Then, in spite of the fact that galaxies in our sample vary by ~ 6 magnitudes in the I band, we obtain a universal function of the normalized galactocentric radius, similar to that set up in PSS, that is able to fit well the double normalized coadded RCs of galaxies, when extrapolated to our much lower masses.

To summarise, we have worked out the ddURC, i.e. an analytical model for the dwarf disks coadded curve, that represents the RC of DD galaxies. This function is given by eqs. 3,5,8 and by eq. 15.

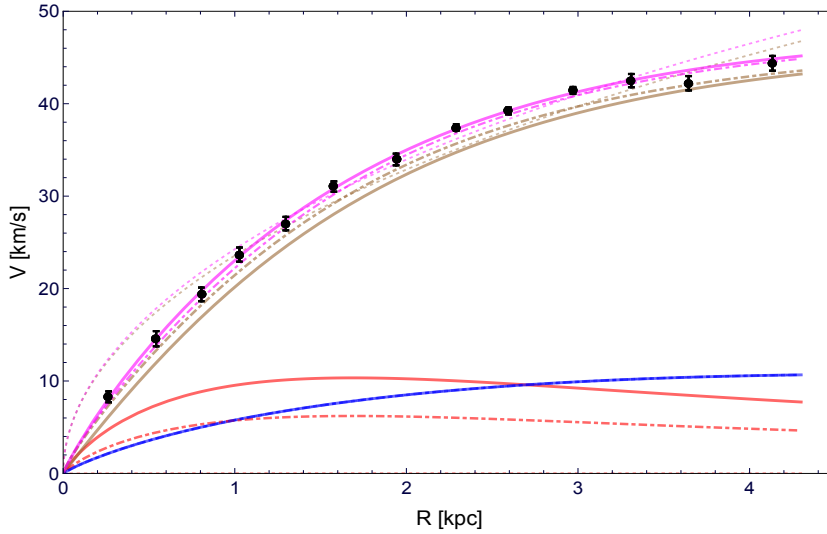


Figure 7. The synthetic RC (filled circles with uncertainties) and URC with its separate dark/luminous contributions (red line: disk; blue line: gas; brown line: halo; pink line: the sum of all components) in case of three DM profiles: the Burkert DM profile (solid lines), NFW profile (dashed lines) and DC14 profile (dot-dashed line).

5 DENORMALISATION OF THE DDURC MASS MODEL

In this section we will construct a URC for the dwarf disk galaxies in the physical units that will cope with the diversity of RCs evident in Fig. (2). In spirals (see PSS) we can easily go back from a double normalized URC $V(R/R_{opt})/V_{opt}$ to a RC expressed in physical units $V(R/kpc, M_I) km/s$, where R_{opt} , V_{opt} and M_I are altogether well correlated. This is not the case for dds where another quantity, the compactness, enters in the above 3-quantity link.

Let us first remind that in every radial bin the residuals do not correlate with the optical velocity of the corresponding galaxy (see Section 3). This implies that the dds structural parameters of the dark and luminous matter have a negligible direct dependence on luminosity/optical velocity different from that inherent to the two normalizations we apply to the individual RCs.

Moreover, given the very small intrinsic scatter of the fiducial double normalized coadded RC and the extremely good fit of the ddURC to it, we can write

$$\frac{M_{D,HI}}{V_{opt}^2 R_{opt}} = \frac{\langle M_{D,HI} \rangle}{\langle V_{opt}^2 \rangle \langle R_{opt} \rangle} \equiv const. \quad (16)$$

Then, we derive, in all objects, a direct proportionality between the halo core radius r_c and the disk scale-length R_D , which is in agreement with the extrapolation of the corresponding relationship in normal spirals of much higher mass (Salucci et al. 2007): $\log(r_c) = 0.47 + 1.38 \log(R_D)$, see Fig. 8.

We also assume that $\frac{V_D^2(R_{opt})}{V_{HI}^2(R_{opt})}$ is constant among galaxies and it equals to the value of the average case $\frac{\langle V_D^2(R_{opt}) \rangle}{\langle V_{HI}^2(R_{opt}) \rangle} \simeq 1.1$.

Consequently with the above assumptions, for each galaxy of the sample, we have

$$M_{DM}(R_{opt}) = (1 - \alpha) V_{opt}^2 R_{opt} G^{-1}, \quad (17)$$

where M_{DM} is the Burkert DM mass inside the optical radius R_{opt} and α is the fraction which baryonic matter contributes to the total circular velocity:

$$\begin{aligned} \alpha &= \frac{\langle V_{HI}^2(R_{opt}) \rangle + \langle V_D^2(R_{opt}) \rangle}{\langle V_{tot}^2(R_{opt}) \rangle} = \\ &= 0.12 \equiv const. \end{aligned} \quad (18)$$

Notice that in some galaxies the fractional contribution to V from the HI disk can be different from the assumed value of ~ 0.06 . However, this has no effect on our investigation. In fact, at the radii where the HI disk is more relevant than the stellar disk, the contribution of the DM halo becomes overwhelming (Evoli et al. 2011).

By simple manipulations of eqs. (16-18) inserting the individual values of R_{opt} , V_{opt} , we get, for each galaxy, the structural parameters of the dark and the luminous matter. In Table 3 we list them along side with their uncertainties obtained from those of the URC mass model given in eq. (15).

5.1 HI gas mass and stellar mass

We now check the validity of the assumptions in the previous subsection. We compare our estimated values of the galaxy HI masses, eq. (16), with those given by K13 (calculated using total H_I flux, for more details see K13). We find:

$$\begin{aligned} \log M_{HIkin} &= (-0.18 \pm 1.20) + \\ &+ (1.01 \pm 0.16) \log M_{HIK13} \end{aligned} \quad (19)$$

with a r.m.s of 0.3 dex. The value of the slope and the small r.m.s., despite the presence of some outliers most probably originating from the large range in luminosities and morphologies of our sample, suggest that M_{HIkin} are good proxies of M_{HIK13} . Therefore, adopting them does not influence any result of this paper.

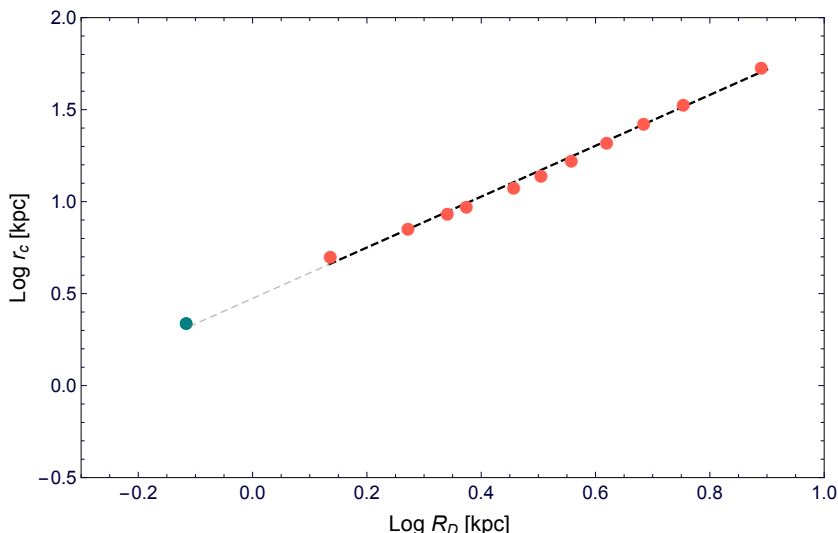


Figure 8. The core radius versus disk scalelength. Red circles represent the values of the URC of normal spirals and green circle represents the best fit values found in the previous section. Black dashed line is a linear fit to the data of the URC of normal spirals and the grey dashed line is the extrapolation of the linear fit to the dwarf disks regime.

We also compare the kinematical derivation of the stellar disk masses for the objects in our sample with those obtained for the same objects from K_S band photometry (provided by K13). Following Bell et al. (2003); McGaugh & Schombert (2015) we adopt a constant mass-to-light ratio of $M/L_K = 0.6 \times M_\odot/L_\odot$ and we report them in Table 3 as $M_D(K_S)$. We find a good correlation between the two estimates:

$$\begin{aligned} \log M_{Dkin} &= (2.58 \pm 1.01) \\ &+ (0.64 \pm 0.13) \log M_{DK_S} \end{aligned} \quad (20)$$

with a r.m.s of 0.4 dex. The two estimates are therefore mutually consistent especially by considering that the kinematical estimate has an uncertainty of 0.3 dex (see Salucci et al. 2008). Let us also notice that in dds the conversion between luminosity and stellar masses is subject to a similarly large systematical uncertainty, especially in actively star-forming galaxies like those present in our sample.

These results, therefore, support well the scheme used in this paper to deal with the luminous components of dds.

Furthermore, we compare our results with Lelli et al. (2016), where the authors analyse a sample of 176 disk galaxies and quantify for them the ratio of baryonic-to-observed velocity. We have, that this ratio, calculated at 2.2 disk scale lengths, is ~ 0.4 . The latter is consistent with values of Lelli et al. (2016), established for a sample of dwarf disk galaxies. Moreover, we found that the value of gas fraction ($f_{gas} \equiv \frac{M_{HI}}{M_{bar}} \sim 0.8$) in our sample is consistent with the value estimated by Lelli et al. (2016), where the authors say that low-luminosity end disk galaxies are extremely gas dominated with $f_{gas} \simeq 0.8 - 1.0$.

5.2 The scaling relations

Let us plot, the central surface density of the DM haloes of our sample, i.e. the product of $\rho_0 r_c$, as a function of B magnitude (see Fig. 9). A constancy of this product has been

found over 18 blue magnitudes and in objects ranging from dwarf galaxies to giant galaxies (e.g Kormendy & Freeman 2004; Gentile et al. 2009; Donato et al. 2009; Plana et al. 2010; Salucci et al. 2012). For the case of dds, in Fig. 9, one can see that most of the objects of our sample fall inside the extrapolation of Donato et al. (2009) relation (see the orange shadowed area of Fig. 9) with a scatter of about 0.3 dex of an uncertain origin.

We now work out the relationships among the various structural properties of the dark and luminous matter of each galaxy in our sample. These will provide us with crucial information on the relation between dark and baryonic matter as well as on the DM itself. Obviously they are necessary to establish a URC for the present sample.

We first derive the galaxy baryonic mass versus halo virial mass relation and compare it with that of normal spiral galaxies (Salucci et al. 2007), see Fig. 10. We take 0.3 dex as $1-\sigma$ error in the baryonic mass (blue shadowed area). Fig. 10 highlights that galaxies of our sample, i.e. dwarf disk objects live in haloes with masses below $5 \times 10^{10} M_\odot$ and above $4 \times 10^8 M_\odot$. A similar result was found by Ferrero et al. (2012), who analysed a sample of dwarf disk galaxies either by using the individual mass modelling or the outermost values of their RCs in order to define the galactic virial mass. In Figure 10, we also show the comparison of our results with the relation of the abundance matching method by Papastergis et al. (2012). Remarkably, for $M_{vir} \lesssim 4 \times 10^{10} M_\odot$, it is inconsistent with the relation found by the abundance matching method (black solid line of Fig. 10) and its extrapolation (black dashed line of Fig. 10). Likewise, $M_{bar} - M_{vir}$ relation found for dwarf disks is significantly shallower than that of the low-mass spirals (joined red circles of Fig. 10).

Furthermore, let us stress that the fit resulting from the baryon-influenced DC14 profile has a lower value of the baryonic mass (yellow dot of Fig. 10). Consequently, it comes quite close to the extrapolation of the abundance matching relation (black dashed line of Fig. 10). However, to investigate properly this issue we should find the relations similar

Table 3. Sample of dd galaxies. Columns: **(1)** galaxy name; **(2)** the stellar disk mass; **(3)** the stellar disk mass using K-band luminosities; **(4)** the gas mass; **(5)** the gas mass listed in Karachentsev et al. (2013); **(6)** the core radius; **(7)** the central density; **(8)** the halo mass; **(9)** compactness of the stellar disk.

Name	M_D $\times 10^7$	$M_D(K_S)$ $\times 10^7$	M_{HI} $\times 10^7$	$M_{HI}(K13)$ $\times 10^7$	r_c	$\log(\rho_0)$	M_h $\times 10^9$	C
—	M_\odot	M_\odot	M_\odot	M_\odot	kpc	g/cm^3	M_\odot	—
(1)	(2)	(3)	(4)	(5)	(6)	(7)	(8)	(9)
UGC1281	12.2	19.9	39.5	22.1	2.93	-23.6	32.2	1.05
UGC1501	15.1	23.9	48.8	38.4	4.32	-23.9	43.8	0.87
UGC5427	4.63	8.28	15.02	3.93	0.76	-22.5	8.85	1.80
UGC7559	5.2	7.21	16.8	13.9	2.46	-23.8	11.8	0.81
UGC8837	14.9	24.4	48.2	29.8	5.40	-24.2	44.4	0.74
UGC7047	3.28	11.4	10.6	15.3	1.34	-23.3	6.50	1.02
UGC5272	16.4	6.58	53.1	23.1	4.14	-23.8	47.8	0.93
DDO52	19.8	14.7	64.3	27.8	4.24	-23.8	59.8	1.0
DDO101	13.8	49.9	44.7	16.0	2.71	-23.4	36.6	1.17
DDO154	4.58	2.33	14.9	25.3	1.98	-23.6	9.99	0.90
DDO168	12.7	8.28	41.1	29.8	2.28	-23.3	32.4	1.28
Haro29	1.26	3.96	4.11	7.65	0.51	-22.6	2.01	1.34
Haro36	3.92	13.8	15.8	14.9	2.84	-23.5	35.0	1.11
IC10	2.31	17.7	8.80	13.3	0.78	-22.8	4.91	1.39
NGC2366	16.4	28.1	53.2	54.2	4.16	-23.8	47.97	0.93
WLM	1.79	2.94	8.23	9.0	1.29	-23.4	4.84	0.94
UGC7603	17.1	53.5	55.6	55.4	3.42	-23.6	48.8	1.09
UGC7861	9.74	97.3	31.6	41.1	1.51	-23.0	22.5	1.53
NGC1560	14.7	31.5	47.6	142.5	3.37	-23.7	40.7	1.03
DDO125	0.60	7.55	1.95	4.02	1.1	-23.8	0.92	0.55
UGC5423	1.66	15.4	5.39	9.2	1.19	-23.5	2.97	0.82
UGC7866	1.90	9.29	6.15	10.6	1.27	-23.5	3.47	0.83
DDO43	3.0	2.44	9.72	9.42	1.35	-23.3	5.88	0.98
IC1613	0.92	7.05	3.0	7.8	1.46	-23.9	1.52	0.54
UGC4483	0.34	0.6	1.11	4.4	0.29	-22.6	4.51	1.12
KK246	2.51	3.96	9.56	15.6	1.40	-23.4	5.79	0.95
NGC6822	2.94	13.1	9.41	18.8	1.32	-23.3	5.65	0.98
UGC7916	9.45	3.79	30.7	35.8	5.80	-24.4	26.2	0.57
UGC5918	10.4	12.3	33.9	23.1	3.88	-23.0	28.2	0.80
AndIV	2.08	0.77	6.76	27.8	1.06	-23.2	3.79	0.99
UGC7232	1.23	4.77	4.0	3.84	0.34	-22.2	1.87	1.75
DDO133	6.85	10.4	22.2	21.1	2.55	-23.7	16.4	0.90
UGC8508	0.77	2.13	2.48	2.65	0.50	-22.8	1.15	1.08
UGC2455	9.93	122.5	32.2	87.9	3.21	-23.8	25.9	0.90
NGC3741	0.36	1.44	1.16	10.1	0.27	-22.4	0.47	1.22
UGC11583	13.5	5.73	43.9	24.8	3.67	-23.8	37.6	0.93

to that described in Section 5. The latter is beyond the scope of this paper and we are going to address this in a future work.

Notice, that there is some discrepancy (irrelevant to the results of this paper) in the baryonic to halo mass relation also at higher masses. The latter is most likely due to the difference of Hubble types in the samples and in the analysis used to obtain these relations.

Then we derive our galaxy baryonic mass versus halo virial mass relation by fitting it with the function of 7 free parameters advocated by Ferrero et al. (2012) :

$$\begin{aligned}
 M_{bar} &= M_{vir} \times A \left(1 + \left(\frac{M_{vir}}{10^{M_1}} \right)^{-2} \right)^\kappa \\
 &\times \left(\left(\frac{M_{vir}}{10^{M_0}} \right)^{-\alpha} + \left(\frac{M_{vir}}{10^{M_0}} \right)^\beta \right)^{-\gamma}, \quad (21)
 \end{aligned}$$

we found $A = 0.070$, $\kappa = 1.80$, $M_1 = 11.36$, $M_0 = 11.59$, $\alpha = 3.43$, $\beta = 0.042$, $\gamma = 1.8$ (purple dashed line of Fig. 10).

The other two relationships which are necessary to establish a URC of dds also in physical units i.e. $R_D - M_{vir}$ or $\rho_0 - r_c$, show a very large scatter (see Fig. 11) as a consequence of the presence of dwarf disk galaxies in the sample (and in the Universe) with almost the same stellar mass (luminosity) but with a different size of their stellar disks. At face value, relationships in Fig. 11 may lead us to exclude the existence of URC in physical units for dwarf disk galaxies. In fact, the large scatter in Fig. 11 requires a new parameter to restore the URC.

Therefore, we proceed and show that the universality is restored by introducing a new parameter, which we call "compactness" C . We define, for galaxies in the (dd) sample, the quantity C as the ratio between the value *predicted* from the measured galaxy disk mass M_D according to the simple

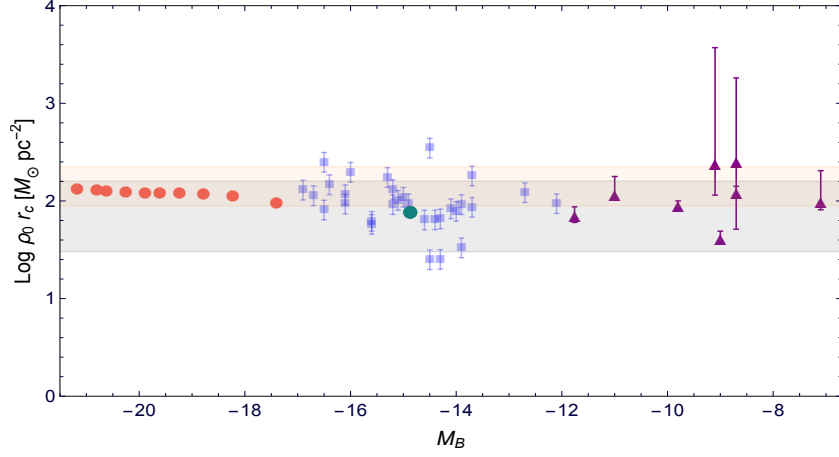


Figure 9. $\rho_0 r_c$ in units of $M_\odot \text{pc}^{-2}$ as a function of a galaxy magnitude for different galaxies and Hubble types. The data are: the Salucci et al. (2012) the URC of normal spiral galaxies (red circles); scaling relation from Donato et al. (2009) (orange shadowed area); Milky Way dSphs (purple triangles) Salucci et al. (2012); dwarf disk galaxies (blue squares-this work, green dot represents the average point), B magnitudes are taking from KK13; empirically inferred scaling relation: $\rho_0 r_c = 75^{+85}_{-45} M_\odot \text{pc}^{-2}$ from Burkert (2015) (grey shadowed area).

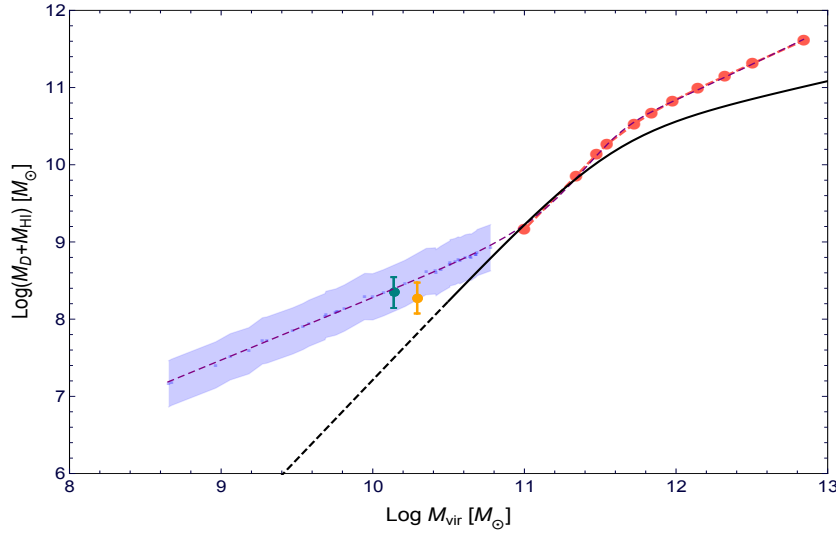


Figure 10. The baryonic mass versus the virial mass for normal spirals (joined red circles) and for the dwarf disks assuming the URC model (blue shadowed area assuming 0.3 dex scatter, the green circle with error bars represents the average point of the region). Yellow dot with error bars is the best fit value for the fiducial RC using DC14 model (see Section 4). Purple dashed line corresponds to the parameterised eq. (21) of the galaxy baryonic mass as a function of halo mass. The abundance matching relation from Papastergis et al. (2012) is shown by black solid line, the region that is extrapolated from the Papastergis et al. (2012) relation is dashed.

linear regression R_D vs M_D of the whole sample and that of R_D measured from photometry. As regard, we find:

$$\log R_D = -3.62 + 0.45 \log M_D. \quad (22)$$

Then, we obtain the following expression of C ,

$$C = \frac{10^{(-3.62 + 0.45 \log M_D)}}{R_D} \quad (23)$$

that obviously describes the differences of the sizes of the stellar disks reduced at a same stellar mass. C varies from -0.27 to 0.26 and its distribution in our sample is listed in Table 3.

By fitting $\log R_D$ to $\log M_{vir}$ with an additional variable $\log C$, we obtain an excellent fit shown in Fig. 12. The model function being,

$$\log R_D = -3.90 + 0.37 \log M_{vir} - 0.94 \log C. \quad (24)$$

this relation just acknowledges the existence of another player in the stellar disk mass-size interplay.

Then we fit $\log \rho_0$ to $\log M_{vir}$ and $\log C$:

$$\log \rho_0 = 12.57 - 0.48 \log M_{vir} + 3.44 \log C. \quad (25)$$

Finally, we fit $\log \rho_0 - \log r_c$ by adding $\log C$ as a free

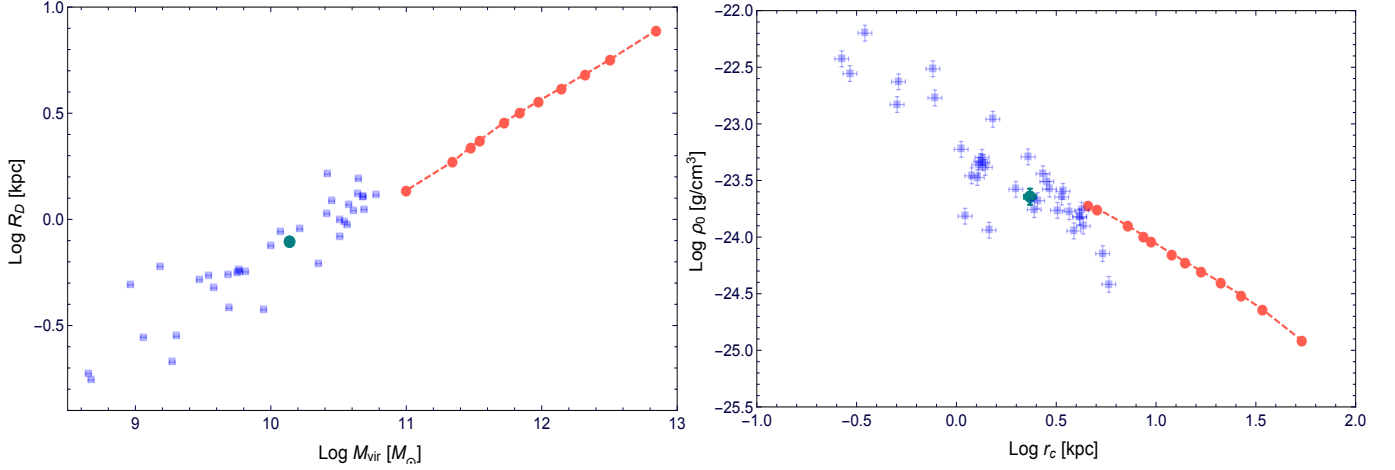


Figure 11. *Left panel:* the disk scalelength versus virial mass. *Right panel:* the central density versus core radius. Red circles represent normal spirals, blue squares with error bars correspond to dwarf disks of this work and the green circle with error bars represents the average point.

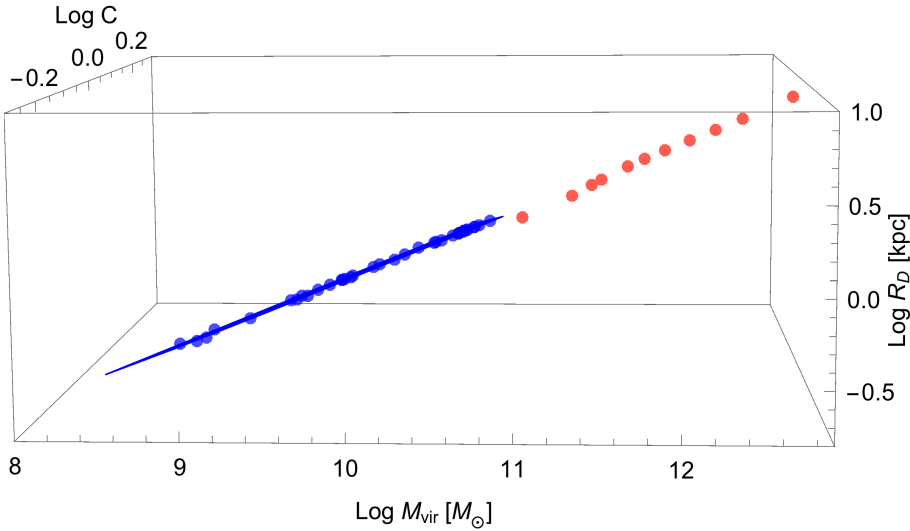


Figure 12. The disk scalelength versus virial mass and the compactness parameter C . Red circles represent normal spirals, blue squares with error bars correspond to dwarf disks of this work and blue line is the result of the fit (for details see text).

parameter. The result of the fit is shown on Fig. 13 and the model function is,

$$\log \rho_0 = -23.19 - 0.93 \log r_c + 2.23 \log C. \quad (26)$$

It is remarkable that a basic property of the stellar disks enters to set the relationship between two DM structural quantities. Therefore, the scatter, which appears in dwarf disks when we try to relate the local properties of either baryonic or DM can be eliminated by using an additional parameter C .

Then, analogously to the compactness of the stellar disk, we define C_{DM} as the compactness of the DM halo. This quantity is the ratio, galaxy by galaxy, between the DM core radius r_c (see column 6 of Table 3) and the pre-

dicted value that we obtain from the simple linear regression between r_c and M_{vir} , which reads:

$$\log r_c = -4.98 + 0.52 \log M_{vir}. \quad (27)$$

Then, we have:

$$C_{DM} = \frac{10^{-4.98+0.52 \log M_{vir}}}{r_c}. \quad (28)$$

We find that the compactness of the stellar disk is closely related to the compactness of the DM halo, see Fig. 14. Consequently, the DM and the stars distributions follow each other very closely. This is extremely remarkable: it may indicate a non standard nature of the dark matter or the fact that baryonic feedbacks ease the cusp core problem

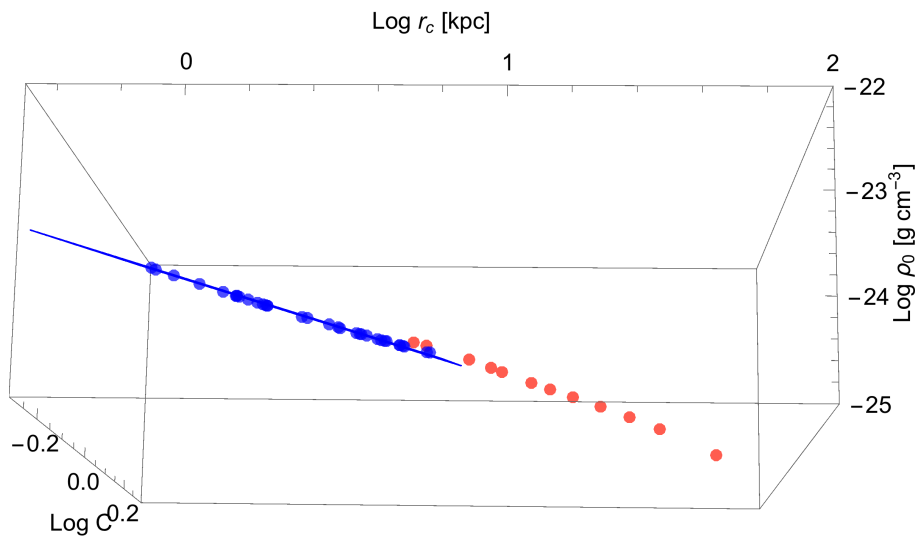


Figure 13. The central density versus core radius and the compactness parameter C . The lines and symbols are as in Fig. 12.

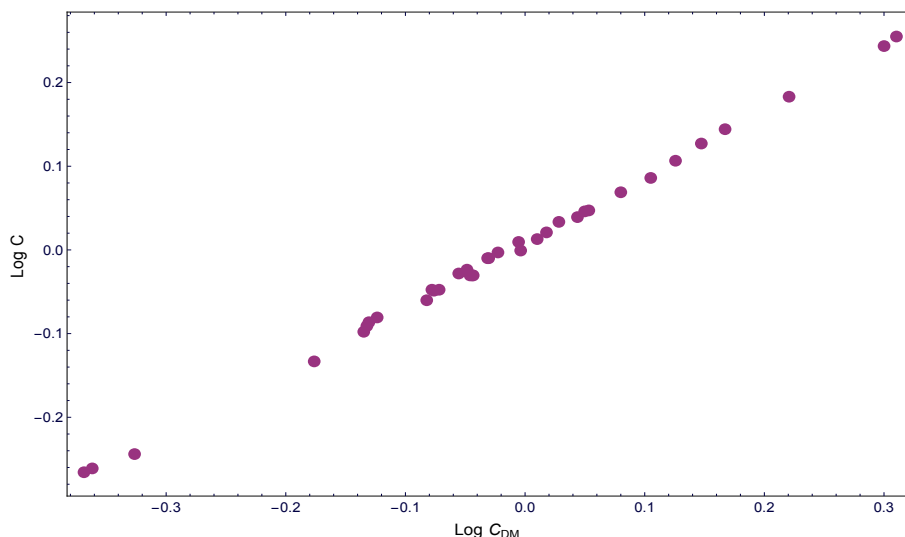


Figure 14. The compactness of the stellar disk versus the compactness of the dark matter halo.

in a WIMP scenario (see, e.g., Teyssier et al. 2013; El-Badry et al. 2016; Dutton et al. 2016; Di Cintio et al. 2016)

Finally, by using eqs. (5,6,8,21,23-26) we derive $V_{ddURC}(R, M_D, C)$ the universal function that describes the dwarf disk RCs in physical units. Differently, from normal Spirals it has 2 parameters, disk mass M_D and concentration C , to account to the diversity of the mass distribution of these galaxies.

6 SUMMARY AND CONCLUSIONS

We have compiled literature data for a sample of dd galaxies in the local volume ($\lesssim 11 Mpc$) with HI and H_α RCs in order to establish their URC in normalized and physical units and to investigate the related dark and luminous matter properties, not yet studied statistically in these galaxies. Our sample spans ~ 2 decades ($\sim 10^6 - 3 \times 10^8 L_\odot$) in luminosity, which coincides with the faint end of the luminosity

function of disk galaxies. In magnitude extension is as large as the whole range of normal spirals usually investigated. The galaxies in the sample are up to ~ 4 magnitudes fainter than the lowest limit in the PSS sample.

We find that, the large variations of our sample in luminosity and morphologies require double normalization, after that we have that all RCs in double normalized units are alike. This implies that the structural parameters of the dark and luminous matter for the galaxies in our sample do not have any explicit dependence from luminosity except those coming from the normalizing process. Additionally, the good agreement of our coadded RC with that of the first PSS's luminosity bin indicates that in such small galaxies the mass structure is already dominated by a dark halo with a density core as big as a stellar disk.

Then by applying to the double normalized rotation curve the standard χ^2 mass modelling of RCs, we tested three DM density profiles. The NFW profile fails to reproduce the coadded curve, while the Burkert and DC14 profiles

show excellent quality fits with $\chi^2_{red} < 1$. This result points towards the cored DM distribution in dwarf disk galaxies. The same conclusion was drawn in the papers on Things and Little Things dwarfs galaxies (see, e.g., [Oh et al. 2011, 2015](#)), where the authors found for their dwarfs much shallower inner logarithmic DM density slopes than those predicted by DM-only (Λ)CDM simulations. The present analysis has the advantages of bigger statistics, but above all, is immune from systematics that can affect the mass modelling of individual galaxies.

We also found, galaxy by galaxy, the values of the dark and luminous matter structural parameters. Surprisingly, a new actor enters the scene of the distribution of matter in galaxies, the compactness of the stellar component, which allows us to establish the ddURC.

As a consequence of the derived mass distributions, there is no evidence for the sharp decline in the baryonic to halo mass relation. Similar result, for dwarf galaxies in the field, was found by [Ferrero et al. \(2012\)](#). However, in DC14 case the estimated baryonic mass is slightly lower than that of the URC mass model, which brings it closer to the abundance matching relation inferred from e.g. [Papastergis et al. \(2012\)](#). The [Di Cintio et al. \(2014\)](#) model has been already tested against observations in works by [Katz et al. \(2016\)](#) and [Pace \(2016\)](#). Although both groups use similar methods, the drawn conclusions are different (see also [Read et al. 2016](#)). Therefore, the consistency level between observations and the (Λ)CDM model of galaxy formation, specifically the abundance matching technique deserves further investigation.

Furthermore, the S-shape of $M_{vir} - M_{bar}$ relation may be interpreted as different physical mechanism occurring along the mass sequence of disk galaxies. Theoretically, it has been shown that the energetics of star formation differs among different galaxies with a characteristic dependence on the halo-to-stellar mass ratio ([Di Cintio et al. 2014](#); [Chan et al. 2015](#)) and possibly also on star formation history ([Oñorbe et al. 2015](#)). Remarkably we also find that the distribution of the stellar component and its DM halo are related.

Finally we recall that the study of the ddURC has lead to the main properties of dark matter in dwarf disks and it will be integrated by future analyses of suitable individual RCs, once they will be available in a sufficient number.

ACKNOWLEDGEMENTS

We would like to acknowledge Luigi Danese and Andrea Lapi for valuable discussions. The authors grateful to the anonymous referees for useful comments and suggestions. We thank Brigitte Greinöcker for language corrections.

REFERENCES

- Begum A., Chengalur J. N., 2004, *A&A*, **424**, 509
- Bell E. F., de Jong R. S., 2001, *ApJ*, **550**, 212
- Bell E. F., McIntosh D. H., Katz N., Weinberg M. D., 2003, *ApJS*, **149**, 289
- Binggeli B., 1994, in Meylan G., Prugniel P., eds, European Southern Observatory Conference and Workshop Proceedings Vol. 49, European Southern Observatory Conference and Workshop Proceedings. p. 13
- Bosma A., 2004, in Ryder S., Pisano D., Walker M., Freeman K., eds, IAU Symposium Vol. 220, Dark Matter in Galaxies. p. 39 ([arXiv:astro-ph/0312154](#))
- Boylan-Kolchin M., Bullock J. S., Kaplinghat M., 2012, *MNRAS*, **422**, 1203
- Brook C. B., et al., 2012, *MNRAS*, **426**, 690
- Burkert A., 1995, *ApJ*, **447**, L25
- Burkert A., 2015, *ApJ*, **808**, 158
- Chan T. K., Kereš D., Oñorbe J., Hopkins P. F., Muratov A. L., Faucher-Giguère C.-A., Quataert E., 2015, *MNRAS*, **454**, 2981
- Dalcanton J. J., Stilp A. M., 2010, *ApJ*, **721**, 547
- Di Cintio A., Brook C. B., Macciò A. V., Stinson G. S., Knebe A., Dutton A. A., Wadsley J., 2014, *MNRAS*, **437**, 415
- Di Cintio A., Brook C. B., Dutton A. A., Macciò A. V., Oñorbe J., Dekel A., 2016, preprint, ([arXiv:1608.01327](#))
- Donato F., et al., 2009, *MNRAS*, **397**, 1169
- Dutton A. A., et al., 2016, *MNRAS*, **461**, 2658
- El-Badry K., Wetzel A., Geha M., Hopkins P. F., Kereš D., Chan T. K., Faucher-Giguère C.-A., 2016, *ApJ*, **820**, 131
- Elbert O. D., Bullock J. S., Garrison-Kimmel S., Rocha M., Oñorbe J., Peter A. H. G., 2015, *MNRAS*, **453**, 29
- Epinat B., et al., 2008, *MNRAS*, **388**, 500
- Evoli C., Salucci P., Lapi A., Danese L., 2011, *ApJ*, **743**, 45
- Ferrero I., Abadi M. G., Navarro J. F., Sales L. V., Gurovich S., 2012, *MNRAS*, **425**, 2817
- Freeman K. C., 1970, *ApJ*, **160**, 811
- Fukugita M., Shimasaku K., Ichikawa T., 1995, *PASP*, **107**, 945
- Garrison-Kimmel S., Boylan-Kolchin M., Bullock J. S., Kirby E. N., 2014, *MNRAS*, **444**, 222
- Gentile G., Salucci P., Klein U., Vergani D., Kalberla P., 2004, *MNRAS*, **351**, 903
- Gentile G., Burkert A., Salucci P., Klein U., Walter F., 2005, *ApJL*, **634**, L145
- Gentile G., Salucci P., Klein U., Granato G. L., 2007, *MNRAS*, **375**, 199
- Gentile G., Famaey B., Zhao H., Salucci P., 2009, *Nature*, **461**, 627
- Gentile G., Baes M., Famaey B., van Acoleyen K., 2010, *MNRAS*, **406**, 2493
- Gentile G., Angus G. W., Famaey B., Oh S.-H., de Blok W. J. G., 2012, *A&A*, **543**, A47
- Gilmore G., Wilkinson M., Kleyna J., Koch A., Evans W., Wyse R. F. G., Grebel E. K., 2007, *Nuclear Physics B Proceedings Supplements*, **173**, 15
- Herrmann K. A., Hunter D. A., Elmegreen B. G., 2013, *AJ*, **146**, 104
- Hunter D. A., Elmegreen B. G., 2004, *AJ*, **128**, 2170
- Hunter D. A., Elmegreen B. G., Oh S.-H., Anderson E., Nordgren T. E., Massey P., Wilsey N., Riabokin M., 2011, *AJ*, **142**, 121
- Hunter D. A., et al., 2012, *AJ*, **144**, 134
- Jarrett T. H., Chester T., Cutri R., Schneider S. E., Huchra J. P., 2003, *AJ*, **125**, 525
- Jungman G., Kamionkowski M., Griest K., 1996, *Phys. Rep.*, **267**, 195
- Karachentsev I. D., Makarov D. I., Kaisina E. I., 2013, *AJ*, **145**, 101
- Karachentsev I. D., Chengalur J. N., Tully R. B., Makarova L. N., Sharina M. E., Begum A., Rizzi L., 2016, *Astronomische Nachrichten*, **337**, 306
- Katz H., Lelli F., McGaugh S. S., Di Cintio A., Brook C. B., Schombert J. M., 2016, preprint, ([arXiv:1605.05971](#))
- Klypin A., Kravtsov A. V., Valenzuela O., Prada F., 1999, *ApJ*, **522**, 82
- Klypin A., Karachentsev I., Makarov D., Nasonova O., 2015, *MNRAS*, **454**, 1798
- Kolb E. W., Turner M. S., 1990, The Early Universe. Frontiers in Physics Vol. 69, Addison-Wesley, Redwood City, CA
- Kormendy J., 1985, *ApJ*, **295**, 73
- Kormendy J., Freeman K. C., 2004, in Ryder S., Pisano D., Walker M., Freeman K., eds, IAU Symposium Vol. 220, Dark Matter in Galaxies. p. 377 ([arXiv:astro-ph/0407321](#))
- Lelli F., Verheijen M., Fraternali F., Sancisi R., 2012, *A&A*, **544**, A145
- Lelli F., Verheijen M., Fraternali F., 2014, *A&A*, **566**, A71
- Lelli F., McGaugh S. S., Schombert J. M., 2016, preprint, ([arXiv:1606.09251](#))
- Lovell M. R., Frenk C. S., Eke V. R., Jenkins A., Gao L., Theuns T., 2014, *MNRAS*, **439**, 300
- Martin M. C., 1998, *A&AS*, **131**, 73
- Mashchenko S., Couchman H. M. P., Wadsley J., 2006, *Nature*, **442**, 539
- McGaugh S., 2014, *Galaxies*, **2**, 601
- McGaugh S. S., Schombert J. M., 2015, *ApJ*, **802**, 18
- Moiseev A. V., 2014, *Astrophysical Bulletin*, **69**, 1
- Moore B., Ghigna S., Governato F., Lake G., Quinn T., Stadel J., Tozzi P., 1999, *ApJ*, **524**, L19
- Navarro J. F., Eke V. R., Frenk C. S., 1996a, *MNRAS*, **283**, L72
- Navarro J. F., Frenk C. S., White S. D. M., 1996b, *ApJ*, **462**, 563
- Noordermeer E., van der Hulst J. M., Sancisi R., Swaters R. S., van Albada T. S., 2007, *MNRAS*, **376**, 1513
- Oñorbe J., Boylan-Kolchin M., Bullock J. S., Hopkins P. F., Kereš D., Faucher-Giguère C.-A., Quataert E., Murray N., 2015, *MNRAS*, **454**, 2092
- Oh S.-H., de Blok W. J. G., Brinks E., Walter F., Kennicutt Jr. R. C., 2011, *AJ*, **141**, 193
- Oh S.-H., et al., 2015, *AJ*, **149**, 180
- Oman K. A., et al., 2015, *MNRAS*, **452**, 3650
- Pace A. B., 2016, preprint, ([arXiv:1605.05326](#))
- Papastergis E., Martin A. M., Giovanelli R., Haynes M. P., 2011, *ApJ*, **739**, 38
- Papastergis E., Cattaneo A., Huang S., Giovanelli R., Haynes M. P., 2012, *ApJ*, **759**, 138
- Papastergis E., Giovanelli R., Haynes M. P., Shankar F., 2015, *A&A*, **574**, A113
- Parodi B. R., Barazza F. D., Binggeli B., 2002, *A&A*, **388**, 29
- Persic M., Salucci P., 1991, *ApJ*, **368**, 60
- Persic M., Salucci P., Stel F., 1996, *MNRAS*, **281**, 27
- Plana H., Amram P., Mendes de Oliveira C., Balkowski C., 2010, *AJ*, **139**, 1
- Pontzen A., Governato F., 2012, *MNRAS*, **421**, 3464
- Pontzen A., Governato F., 2014, *Nature*, **506**, 171
- Read J. I., Gilmore G., 2005, *MNRAS*, **356**, 107
- Read J. I., Iorio G., Agertz O., Fraternali F., 2016, preprint, ([arXiv:1601.05821](#))
- Rubin V. C., Burstein D., Ford Jr. W. K., Thonnard N., 1985, *ApJ*, **289**, 81
- Salucci P., 2001, *MNRAS*, **320**, L1
- Salucci P., Burkert A., 2000, *ApJ*, **537**, L9
- Salucci P., Persic M., 1997, in Persic M., Salucci P., eds, Astronomical Society of the Pacific Conference Series Vol. 117, Dark and Visible Matter in Galaxies and Cosmological Implications. p. 1 ([arXiv:astro-ph/9703027](#))
- Salucci P., Lapi A., Tonini C., Gentile G., Yegorova I., Klein U., 2007, *MNRAS*, **378**, 41
- Salucci P., Yegorova I. A., Drory N., 2008, *MNRAS*, **388**, 159
- Salucci P., Wilkinson M. I., Walker M. G., Gilmore G. F., Grebel

- E. K., Koch A., Frigerio Martins C., Wyse R. F. G., 2012, *MNRAS*, **420**, 2034
- Sharina M. E., et al., 2008, *MNRAS*, **384**, 1544
- Simard L., Trevor Mendel J., Patton D. R., Ellison S. L., McConnell A. W., 2011, *VizieR Online Data Catalog*, **219**
- Simon J. D., Bolatto A. D., Leroy A., Blitz L., Gates E. L., 2005, *ApJ*, **621**, 757
- Stinson G. S., Brook C., Macciò A. V., Wadsley J., Quinn T. R., Couchman H. M. P., 2013, *MNRAS*, **428**, 129
- Swaters R. A., Sancisi R., van Albada T. S., van der Hulst J. M., 2009, *A&A*, **493**, 871
- Teyssier R., Pontzen A., Dubois Y., Read J. I., 2013, *MNRAS*, **429**, 3068
- Tolstoy E., Hill V., Tosi M., 2009, *ARA&A*, **47**, 371
- Tonini C., Lapi A., Shankar F., Salucci P., 2006, *ApJ*, **638**, L13
- Verheijen M., de Blok E., 1999, *Ap&SS*, **269**, 673
- Vogelsberger M., Zavala J., Simpson C., Jenkins A., 2014, *MNRAS*, **444**, 3684
- Weinberg D. H., Bullock J. S., Governato F., Kuzio de Naray R., Peter A. H. G., 2013, preprint, ([arXiv:1306.0913](https://arxiv.org/abs/1306.0913))
- Weldrake D. T. F., de Blok W. J. G., Walter F., 2003, *MNRAS*, **340**, 12
- White S. D. M., Negroponte J., 1982, *MNRAS*, **201**, 401
- Yegorova I. A., Salucci P., 2007, *MNRAS*, **377**, 507
- Yoshino A., Yamauchi C., 2015, *MNRAS*, **446**, 3749
- Zavala J., Jing Y. P., Faltenbacher A., Yepes G., Hoffman Y., Gottlöber S., Catinella B., 2009, *ApJ*, **700**, 1779
- de Blok W. J. G., Bosma A., 2002, *A&A*, **385**, 816
- de Vega H. J., Sanchez N. G., 2013, preprint, ([arXiv:1304.0759](https://arxiv.org/abs/1304.0759))
- de Vega H. J., Moreno O., Moya de Guerra E., Ramón Medrano M., Sánchez N. G., 2013, *Nuclear Physics B*, **866**, 177
- de Vega H. J., Salucci P., Sanchez N. G., 2014, *MNRAS*, **442**, 2717
- van Zee L., 2001, *AJ*, **121**, 2003

APPENDIX A: SAMPLE OF ROTATION CURVES

In Fig A we show the rotation curves of all observed galaxies used in our analyses, i.e. the same galaxies as appear in Table 1. We note that rotation curves of UGC1501, UGC5427, UGC8837, UGC5272, IC10, KK149 and UGC3476a are not extended to $3.2 R_D$ (the vertical dashed grey line of Fig. A indicates the position of $3.2 R_D$ for each galaxy), therefore, in order to know the value of the circular velocity at these radii we made extrapolations.

APPENDIX B: COMPARISON OF THE DDURC AND THE URC OF PSS

In the left panel of Fig. B.1, as already discussed in Section 3, we plot our coadded double normalized RC (black stars) alongside with that of the PSS's four luminosity bins. In this figure the joined red dots correspond to the 1st luminosity bin, the joined green squares correspond to the 6th luminosity bin, the joined orange diamonds to the 9th luminosity bin and the joined pink triangles correspond to the 11th luminosity bin with inside 40, 70, 40 and 16 normal spirals, respectively (see Fig. A1 of PSS). We realise that the coadded RC of the 1st PSS bin and synthetic dd RC have very similar profiles. However, the ddURC appears to be slightly less concentrated than that of the 1st luminosity bin of PSS. The latter might indicate the continuation

of the trend found in PSS, which states that the shape of RCs changes with luminosity. Therefore, in order to check whether we have this trend inside our sample we divided it on 3 subsamples in the following way: the most luminous, least luminous, and the middle half. Then we binned radially each subsample in the same way as described in Section 3. The data in the radial bins of each subsample are presented in Table B1. Furthermore, in the right panel of Fig. B.1 we compare the synthetic RC of the whole dd sample with 3 synthetic RCs of the above defined subsamples. All 4 RCs agree within their uncertainties and we do not find any trend of the shape of the RCs with luminosity. However, a weak trend is impossible to reveal. In fact the small number of galaxies in each bin induce some shot noise. Therefore, in order to further investigate this we need twice as many objects.

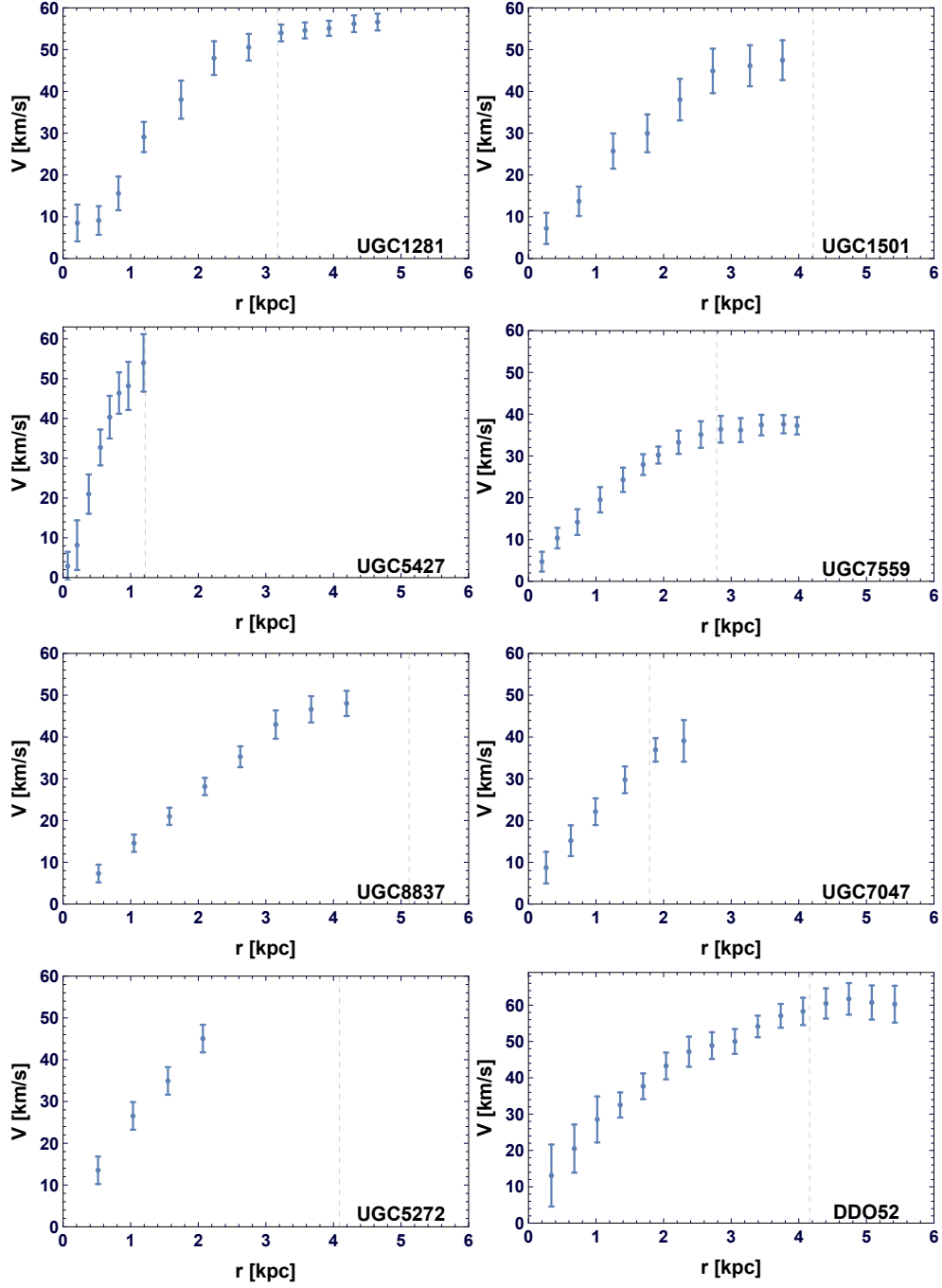
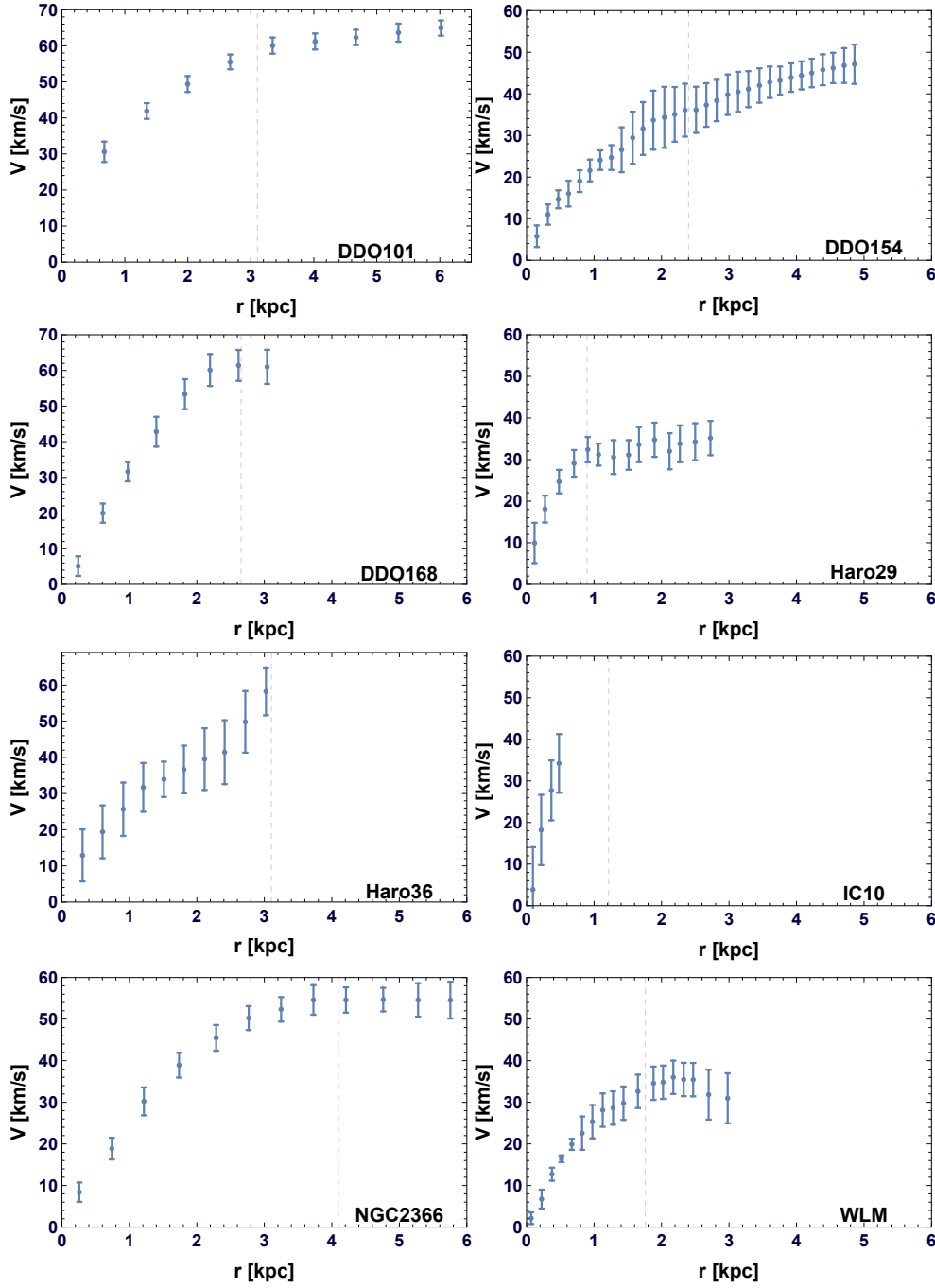


Figure A.2. Individual RCs. Here the R_{opt} are indicated by dashed vertical lines.

Figure A.2 – *continued*

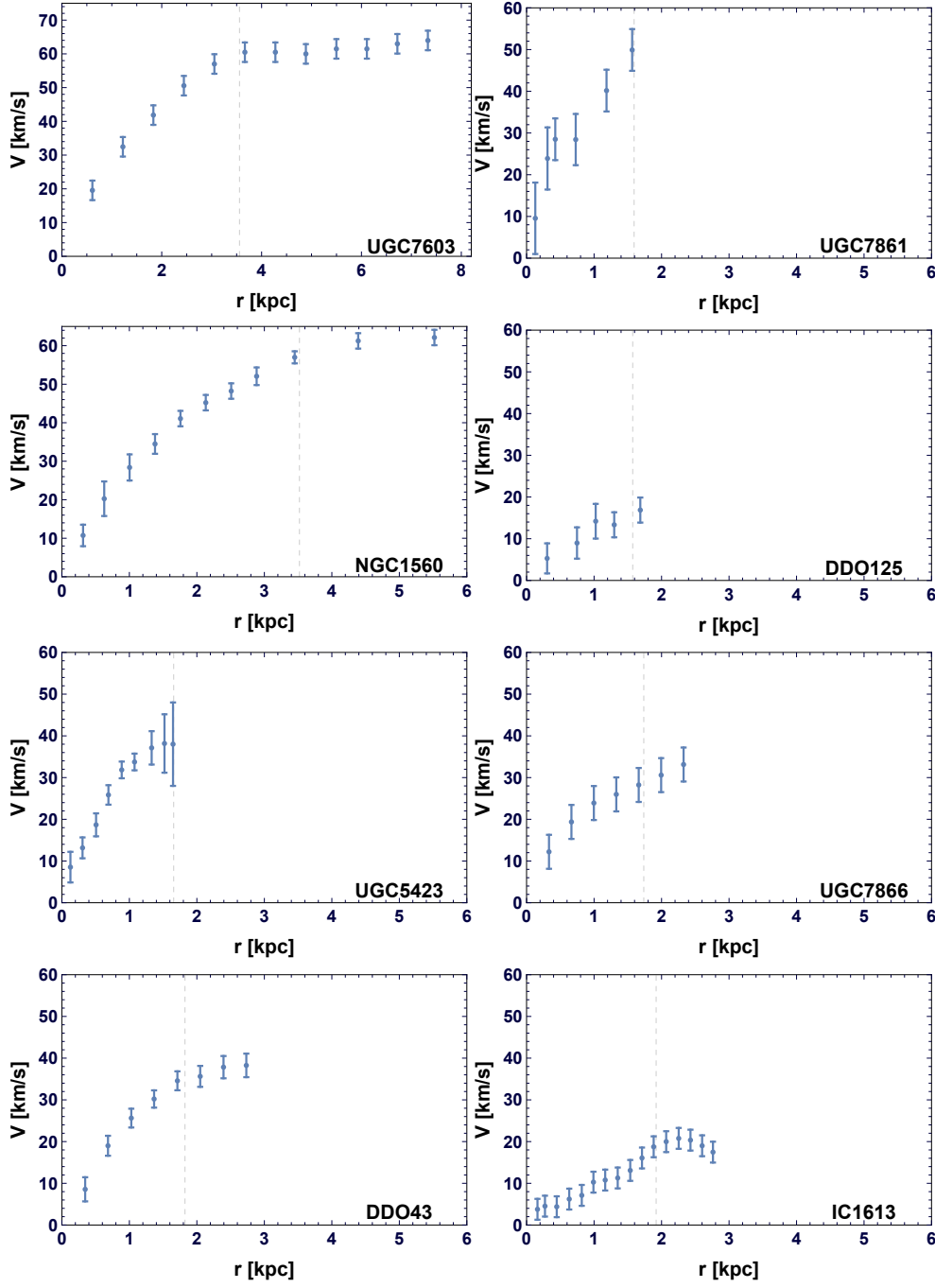
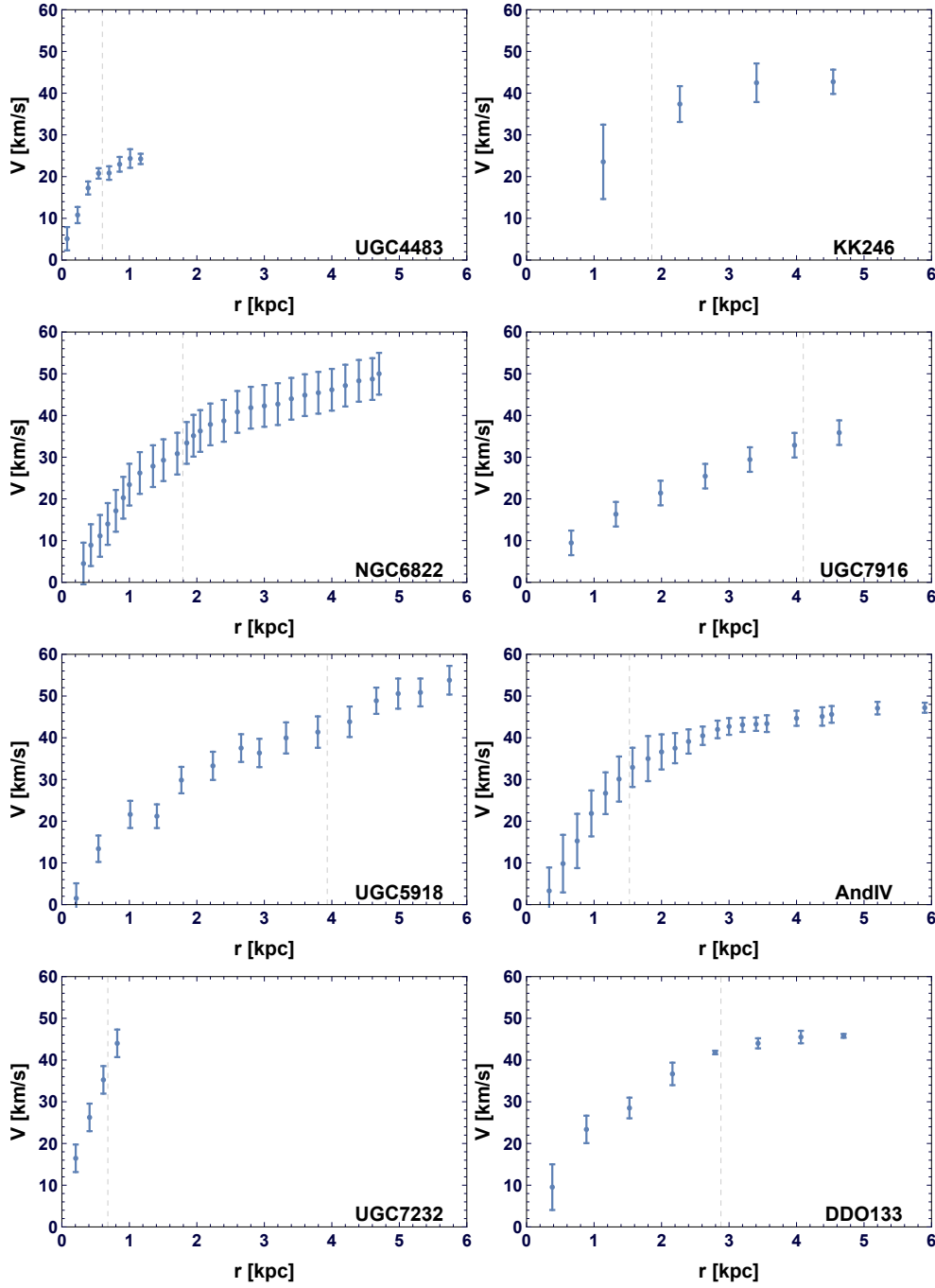


Figure A.2 – *continued*

Figure A.2 – *continued*

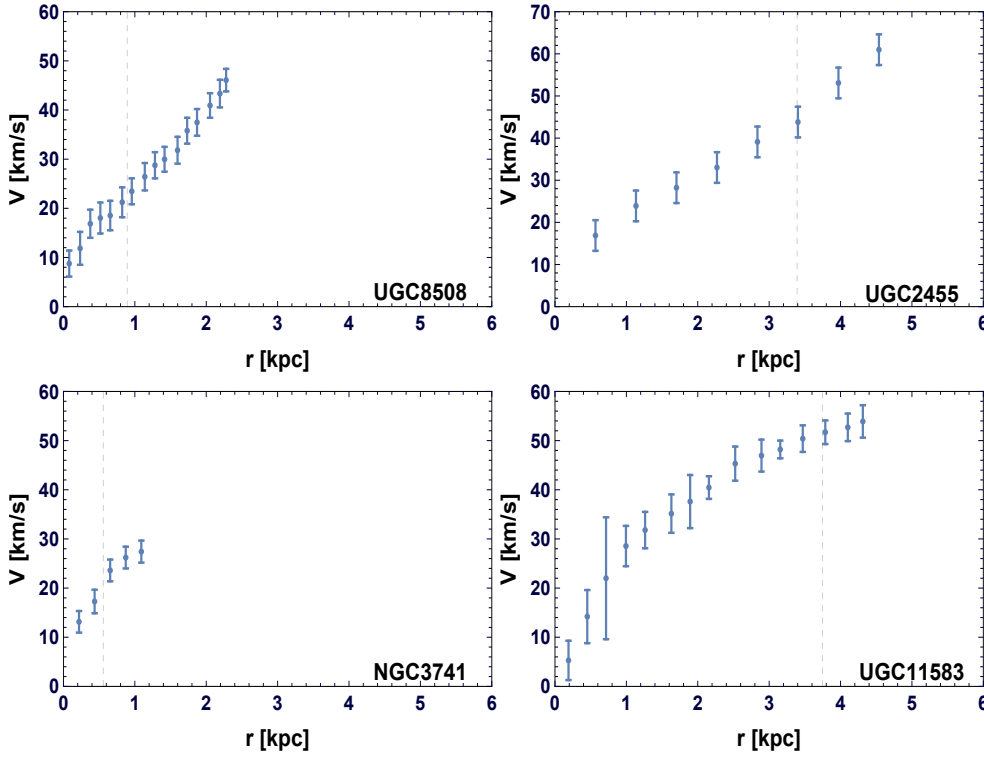
Figure A.2 – *continued*

Table B1. Data in the radial bins of 3 subsamples, ordered from least to most luminous. Columns: (1) bin number; (2) number of data points; (3) the central value of a bin; (4) the average coadded weighted normalized rotation velocity; (5) r.m.s. on the average coadded rotation velocity.

i	N	r_i	v_i	dv_i	N	r_i	v_i	dv_i	N	r_i	v_i	dv_i
(1)	(2)	(3)	(4)	(5)	(2)	(3)	(4)	(5)	(2)	(3)	(4)	(5)
1	9	0.10	0.23	0.030	11	0.11	0.20	0.025	11	0.10	0.20	0.025
2	11	0.25	0.41	0.040	10	0.22	0.35	0.040	12	0.21	0.38	0.024
3	11	0.41	0.59	0.020	12	0.35	0.48	0.033	12	0.33	0.56	0.031
4	8	0.55	0.73	0.011	10	0.48	0.60	0.037	10	0.45	0.65	0.027
5	16	0.70	0.81	0.019	11	0.58	0.70	0.023	15	0.60	0.80	0.018
6	11	0.90	0.95	0.014	11	0.72	0.80	0.028	13	0.77	0.89	0.025
7	13	1.10	1.01	0.013	9	0.83	0.86	0.028	13	0.94	0.96	0.014
8	8	1.27	1.09	0.017	11	0.98	0.97	0.013	8	1.10	1.02	0.016
9	12	1.49	1.11	0.025	8	1.11	1.01	0.013	9	1.28	1.06	0.032
10	7	1.73	1.15	0.052	8	1.23	1.07	0.013	7	1.49	1.04	0.016
11	6	1.92	1.25	0.054	7	1.37	1.07	0.025	7	1.80	1.09	0.025
12	—	—	—	—	3	1.45	1.11	0.088	—	—	—	—
13	—	—	—	—	5	1.62	1.15	0.023	—	—	—	—
14	—	—	—	—	2	1.91	1.11	0.040	—	—	—	—

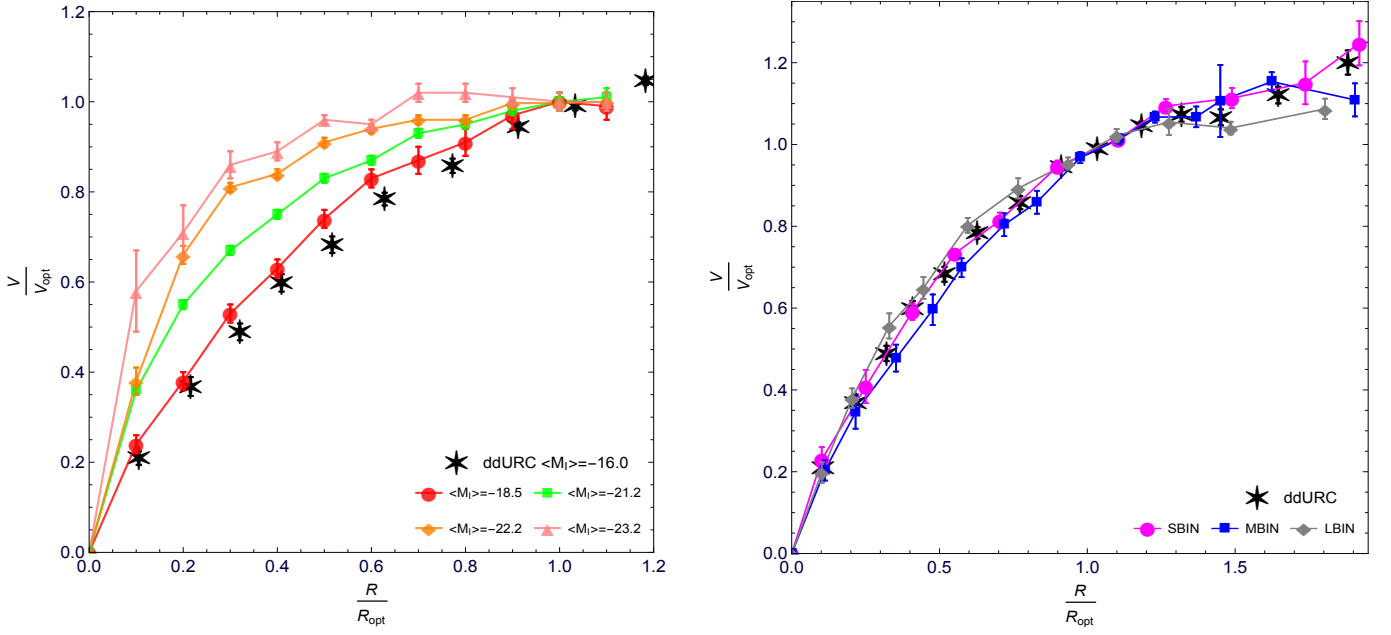


Figure B.1. *Left panel:* joined curves indicate the URC in normalized units of 4 luminosity bins of PSS. *Right panel:* the URC in normalized units of 3 subsamples of dwarf disk galaxies (SBIN-smallest bin; MBIN-mean bin; LBIN-largest bin). Black stars indicate the synthetic RC of the whole sample of dwarfs disk galaxies.